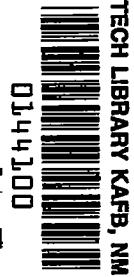


NACA RM L57B07

7749



Reg # 131  
APR 2 1957



# RESEARCH MEMORANDUM

A TRANSONIC INVESTIGATION OF THE MASS-FLOW AND PRESSURE  
RECOVERY CHARACTERISTICS OF SEVERAL  
TYPES OF AUXILIARY AIR INLETS

By John S. Dennard

Langley Aeronautical Laboratory  
Langley Field, Va.

CLASSIFIED DOCUMENT

This material contains information affecting the National Defense of the United States within the meaning of the espionage laws, Title 18, U.S.C., Secs. 793 and 794, the transmission or revelation of which in any manner to an unauthorized person is prohibited by law.

NATIONAL ADVISORY COMMITTEE  
FOR AERONAUTICS

WASHINGTON

April 10, 1957

~~CONFIDENTIAL~~



## NATIONAL ADVISORY COMMITTEE FOR AERONAUTICS

## RESEARCH MEMORANDUM

A TRANSONIC INVESTIGATION OF THE MASS-FLOW AND PRESSURE  
RECOVERY CHARACTERISTICS OF SEVERAL  
TYPES OF AUXILIARY AIR INLETS

By John S. Demard

## SUMMARY

Several basic inlet shapes have been tested through a Mach number range from 0.55 to 1.3 to determine their mass-flow and pressure recovery characteristics when operated as auxiliary inlets. Results indicate that, for flush inlets, the inclination of the inlet axis is the major geometric parameter influencing recovery and the smaller angles with respect to the surface offer decidedly superior performance. For simple flush openings, a circular or low width-depth ratio rectangular opening offers slight advantages over a higher width-depth ratio rectangular opening. Boundary-layer fences for low width-depth ratio inlets are advantageous in increasing the maximum mass-flow rate and pressure recovery at high mass-flow rates. For low mass-flow rates, the NACA submerged inlet with diverging wall ramp offers improved pressure recoveries. A circular scoop inlet with its inner wall tangent to the surface surpassed all flush inlets tested in regard to both total-pressure recovery and maximum mass-flow ratio. The performance of the scoop inlet and all flush inlets with inclined axis deteriorated as the axis was yawed with respect to the stream direction.

## INTRODUCTION

The growing complexity of modern aircraft with much electronic equipment which requires air for cooling, increased requirements for cabin or cockpit ventilation, problems of matching engine and inlet air-flow rates, and the increased use of suction slots for boundary-layer control systems has created a demand for information on the flow characteristics of auxiliary inlets in the transonic speed range. Numerous large-scale inlet investigations have been conducted in this speed range, but except at low subsonic speeds there is little experimental material available whereby the designer may obtain the necessary mass-flow and pressure recovery characteristics of inlets which must induct large amounts of air from within the boundary layer.

~~CONFIDENTIAL~~

The inlet models of the present investigation ranged from flush thin plate inlets to a scoop. Flush circular inlets followed by straight ducts the length-diameter ratios of which varied from 0 to 10 were inclined to the surface at angles from  $15^\circ$  to  $90^\circ$ ; the yaw angle for several of the inlets was varied from  $0^\circ$  to  $60^\circ$ . Rectangular inlets with various inclination angles, width-depth ratios, and ramp approaches were also tested. The Mach number range was from 0.55 to 1.3 and mass-flow rates were varied from 0 to choke. Inlet mass-flow ratios are presented as a function of the required pressure drop and of the total-pressure recovery.

## SYMBOLS

a	velocity of sound, ft/sec
D	hydraulic diameter of inlet, in.
H	total pressure, lb/sq ft
L	length of inlet duct (constant area), in.
$\frac{m_i}{m_0}$	ratio of mass flow through inlet to mass flow in free-stream tube of area equivalent to cross-sectional area of inlet
M	Mach number, $U/a$
n	boundary-layer profile exponent, $\frac{u}{U} = \left(\frac{y}{\delta}\right)^{\frac{1}{n}}$
p	static pressure, lb/sq ft
$\Delta p$	static pressure differential, $p_\infty - p_1$
q	dynamic pressure, $\frac{1}{2}\rho U^2$ , lb/sq ft
u	local velocity in boundary layer, ft/sec
U	free-stream velocity, ft/sec
x	distance measured downstream from inlet lip, in.
y	distance measured from surface to point of local velocity u in boundary layer, in.
$\delta$	boundary-layer thickness measured to point where $u/U = 1.0$ , in.

- $\theta$  inclination angle of inlet axis, deg  
 $\psi$  yaw angle of inlet axis, deg  
 $\phi$  ramp angle, deg

## Subscripts:

- $i$  inlet conditions measured at downstream end of constant-area throat  
 $\infty$  free-stream conditions measured outside of boundary layer

## APPARATUS AND METHODS

## Apparatus

The general arrangement of the test setup is shown in the line drawing of figure 1. Air is supplied through the entrance bell at the left at a maximum pressure of 2 atmospheres absolute from a centrifugal blower without benefit of aftercooling or drying. Air from the entrance bell flows through the slotted test section which consists of parallel walls 17 inches long and  $4\frac{1}{2}$  inches high by  $6\frac{1}{4}$  inches wide and exhausts through a 1.7:1 area ratio diffuser to the atmosphere. The lower wall of the test section was slotted so that one-fifth of the wall area was open. This slotted wall opened into a plenum from which air could be withdrawn by an auxiliary vacuum pump; a valve in the auxiliary pump line determines the rate at which air is removed and thus controls the speed for  $M_\infty > 1$ . The Mach number distributions for this test section are discussed in reference 1. The inlet models were mounted on the solid tunnel wall opposite the slotted wall and centered in one face of a cylindrical settling chamber which has a diameter of  $5\frac{1}{4}$  inches, and a length of  $9\frac{1}{2}$  inches and is located 6 inches downstream of the beginning of the slots. A screen spanned this chamber at a station 3 inches above the inlet. Downstream of the screen, the air flowed through a calibrated venturi. A valve in the exhaust line controlled the mass flow withdrawn from the inlet and the system was aspirated by an auxiliary vacuum pump.

The free-stream total pressure and temperature were measured in the upstream duct and the static pressure was measured in the settling chamber. Other test-section pressure instrumentation included static-pressure orifices in the venturi and a calibrated static-pressure orifice in the plenum.

A sketch showing typical examples of the models tested and the range of variables investigated is shown as figure 2. The inlets tested had circular and rectangular shapes. The circular inlets included inlets with ducts of varying length-diameter ratio ( $L/D$ ), thin-plate inlets, circular flush inclined inlets, and a scoop inlet. The rectangular inlets were flush and had varying inclination angles and width-depth ratios (where depth is measured from the inlet lip perpendicular to the duct axis).

Four of the rectangular inlets were instrumented with static-pressure tubes along the center line of the ramp and through the length of the inlet duct. Figure 3 is a photograph showing several of the inclined rectangular inlets, some with modifications to the ramp, and the circular scoop.

The pressure at the downstream end of the inlet constant-area duct was assumed to be equal to the settling-chamber static pressure. This assumption, which has long been recognized as valid for subsonic flows and which is the basis for most nozzle flow and orifice flow measurements, was verified during the test program by a comparison between the downstream throat static pressure (where available) and the settling chamber static pressure for unchoked inlet operation. This pressure would correspond to the static pressure at the entrance to a diffuser if such were used. The total pressure  $H_1$  is calculated from the measured mass-flow rate and the static pressure with the assumption of uniform velocity distribution at the exit of the constant-area duct. The test-section Mach number is determined by means of the calibrated plenum static-pressure orifice and the upstream total pressure.

Pressures were read to a reading accuracy of  $\pm 1$  millimeter of mercury and this accuracy gives errors in the computed data as follows:

Quantity	Maximum Error
$\frac{p}{H_\infty}$ . . . . .	0.002
$\frac{H_\infty - p}{H_\infty}$ . . . . .	0.002
$\frac{p_\infty - p_1}{q_\infty}$ . . . . .	0.006
$\frac{m_1}{m_0}$ . . . . .	0.008
M . . . . .	0.004
$\frac{H_1}{H_\infty}$ . . . . .	0.009

### Tests and Methods

When the tests were conducted, the inlet air flow was varied from zero to its maximum value for each of several constant values of Mach number ranging from 0.55 to 1.3. The settling-chamber static pressure, free-stream total pressure and total temperature, plenum-chamber static pressure, and mass-flow data were recorded simultaneously. Ramp static pressures were measured on models where pressure-orifice instrumentation was available.

The Reynolds number of these data range from  $3.45 \times 10^6$  per foot at a Mach number of 0.55 to  $7.0 \times 10^6$  per foot at a Mach number of 1.3.

### RESULTS AND DISCUSSION

Auxiliary inlets are usually required to operate in a surface on which the boundary-layer thickness is comparable to the dimensions of the inlet. For these tests the boundary-layer velocity profile and thickness varied with Mach number as shown in figure 4. The profiles indicate a turbulent boundary layer at all Mach numbers. The exponent  $n$  often used to describe the shape of the boundary-layer increases from 5.5 to 8 as the Mach number varies from 0.55 to 1.3. The boundary-layer thickness, defined as the point where  $u/U = 1.0$ , varies from 0.15 inch to 0.115 inch; this variation is linear from  $M = 0.7$  to  $M = 1.3$ .

#### Inlet Performance

The inlet performance data in this paper are presented in three forms: the inlet pressure differential  $H_\infty - p_1$ , the inlet static-pressure differential  $p_\infty - p_1$ , and the inlet total-pressure ratio  $H_1/H_\infty$ . Since these inlets may be located on the airframe in regions where local velocities and pressures are different from those in the free stream, the values of  $M_\infty$  presented herein should be regarded as local Mach numbers in order to apply the results of this investigation.

Inlet pressure differential.- Figure 5 presents the ratio of the inlet pressure differential to stream stagnation pressure  $\frac{H_\infty - p_1}{H_\infty}$  as a function of the inlet mass-flow ratio. This pressure-drop parameter will be particularly useful in designing installations where a diffuser follows the inlet, since the diffuser inlet pressure will correspond to  $p_1$ . However, it is expected that this parameter may be acutely sensitive to variations in the boundary-layer thickness. The curves,

presented for constant Mach number, are characterized by an increase in the inlet pressure differential as the mass flow increases, the rate of change being strongly dependent upon the inlet geometry. Increasing Mach number increases the necessary inlet pressure differential for any given value of mass-flow ratio as indicated by the separation of the curves. The dashed line in each instance indicates the mass-flow ratio for which the indicated inlet Mach number is 1.0. This dotted line is defined as the choke line. For inlets with low inclination angles (figs. 5(b), 5(e), 5(f), and 5(g)) the inlet pressure differential was nearly constant up to mass-flow ratios corresponding to choke for a given  $M_\infty$ ; these inlets would be expected to have a relatively high total-pressure ratio.

Inlet static-pressure differential.- In the second presentation (fig. 6), the inlet static-pressure differential  $p_\infty - p_1$  or  $\Delta p$  is expressed in terms of  $q_\infty$  and is plotted as a function of the mass-flow ratio. These curves are directly comparable with the inlet characteristics in reference 2 and to the perforated-plate characteristics of reference 3. These results are directly applicable to selection of porosity requirements for perforated-tunnel calculations when a given Mach number distribution has been specified. For any given flush inlet configuration, the inlet static-pressure differential at zero mass flow is very nearly constant for all Mach numbers. For the inlets with low inclination angles  $\Delta p/q_\infty$  remains constant over a wide range of mass-flow ratio. For all test configurations,  $\Delta p/q_\infty$  increases as the mass flow approaches its limiting or choking value. Since the allowable contraction ratio before choking occurs is greater for low Mach numbers than it is for Mach numbers near 1.0, it would be expected that the mass-flow ratio would reach higher values for low Mach numbers.

For the scoop inlet (fig. 6(h)), the individual curves follow generally the same pattern as that for the flush inlets; the curves at various Mach numbers are separated further at low mass-flow ratios and cross over near  $\frac{\Delta p}{q_\infty} = 0$ . The separation noted here is due to the compressibility factor  $F_c$ . This factor is equal to  $\frac{H - p}{q}$  and, for this scoop inlet, which is essentially a total-pressure tube when operated at a mass-flow ratio of zero, the inlet static-pressure differential is equivalent to  $-F_c$ . As the mass-flow ratio increases, this correlation becomes less accurate; nevertheless, the general position of the curves relative to one another persists until the inlet mass-flow ratio approaches its choke value.

Inlet total-pressure ratio.- The third presentation (fig. 7) which will form the basis for the bulk of the discussion to follow is the ratio of the inlet total pressure to the free-stream total pressure. The curves

presented here have been faired to match those of figure 5 which, in turn, were faired as families by cross plotting. Restriction of test points to those for which the indicated Mach number at the downstream end of the duct was less than or equal to 1.0, that is, unchoked inlet flow, has resulted in some curves being presented for which there is only one test point. The total-pressure ratio always decreases with increasing Mach number but the variation of  $H_1/H_\infty$  with  $m_1/m_0$  is dependent upon the inlet configuration and orientation with respect to the stream. The inclined inlets exhibit a rising total-pressure ratio with increasing mass-flow ratio up to a point near choke; thereafter, as  $m_1/m_0$  increases, the pressure recovery falls. This increasing recovery is probably due to the ingestion of air from further out in the stream where the total pressure is higher than in the boundary layer. As the inlet approaches a choked condition, local accelerations and friction become increasingly important and the total-pressure ratio decreases. The flush inlets which have their axes more nearly perpendicular to the surface require greater turning angles and, therefore, incur higher losses; for these inlets the pressure recovery decreases throughout the flow range at all except the lowest speeds. Intermediate configurations may be found wherein the total pressure remains essentially constant throughout the unchoked mass-flow range for a given Mach number.

The curves of figure 7 have been cross plotted at constant mass-flow ratios in figure 8 which shows the variation of total-pressure ratio with Mach number for several geometric variables. The symbols do not represent actual test-data points but were obtained from cross fairing. Solid symbols indicate the Mach number and total-pressure ratio corresponding to choking at the particular mass-flow ratios involved. Absence of a solid symbol indicates that choking did not occur in the Mach number range of these tests for that particular mass-flow ratio. Lines representing the ratio of static pressure to total pressure in the free stream are drawn on all figures. These lines represent the pressure which would be measured by a wall static-pressure orifice and are observed to be in fair agreement with the measured pressures at  $\frac{m_1}{m_0} = 0$  throughout most of the Mach number range.

#### Flush Circular Inlets

Effect of L/D.- The pressure recovery of a series of circular inlets followed by a straight duct set perpendicular to the surface is presented as a function of stream Mach number in figure 8(a). These inlets had a diameter of 0.375 inch which is 2.88 times the boundary-layer thickness at a Mach number of 1.0. At all mass-flow ratios for which data are presented,  $H_1/H_\infty$  decreases with increasing Mach number and the slope of the curves increases with mass-flow ratio.

It is observed that the thin-edged inlets ( $L/D = 0$  to  $L/D = 1.0$ ) are generally inferior to those of higher  $L/D$ . The optimum duct length, although not well defined, lies in the range from 3 diameters to  $7\frac{1}{2}$  diameters. The improvement due to long ducts may be due largely to reattachment of the flow to the duct walls after the sharp turn at the inlet and the resultant diffusion of the flow into the settling chamber. These results are in agreement with the transonic results of reference 3 where it was reported that the pressure recovery increased as  $L/D$  is increased from  $1/4$  to 4.

Effect of  $\theta$ .— The effects of inclination of the inlet axis for flush circular inlets are presented in figure 8(b) where the pressure recovery is presented as a function of  $M_o$  for values of  $\theta$  from  $15^\circ$  to  $90^\circ$ .

At  $\frac{m_1}{m_0} = 0$ , the measured recovery for  $\theta = 90^\circ$  approximates the stream static-pressure curve very closely but, as the duct axis is inclined, the recovery increases rapidly especially at low values of  $\theta$ . A comparison of the various groups of curves shows that the pressure recovery of the  $15^\circ$  inlet increases with mass-flow ratio whereas the opposite is true for the  $90^\circ$  inlet. This was also observed in the curves of figure 7(b). The increase in total pressure resulting from the ingestion of increasingly higher pressure air from the areas higher in the boundary layer may be calculated for an idealized condition of zero cross flow by the methods of reference 4. For a  $15^\circ$  inlet the measured total pressures closely follow the predicted values at low Mach numbers and agree in form at higher Mach numbers but, because of local accelerations, shocks, and shock—boundary-layer interaction, differ in magnitude.

As the inlet inclination is increased above  $15^\circ$ , the upstream turning becomes less efficient and air flows into the inlet from the sides; thus, the total-pressure ratio and the maximum mass-flow rate decrease. All curves for these flush circular inlets show a rapidly decreasing total pressure at mass-flow ratios near choke. This condition is probably the result of the increased friction losses as the inlet velocity increases, the increased momentum losses as air flows over the sharp lips as was reported in reference 5, and nonuniformity of the velocity distribution at the discharge of the inlets.

Effect of yaw angle.— The flush circular inlet with  $\theta = 15^\circ$  and  $L/D = 5$  was tested at yaw angles of  $30^\circ$  and  $60^\circ$  in addition to the unyawed position. These results are presented in figure 8(c). There is a striking similarity between these curves and those for the inlets of figure 8(b) where the axis became nearly normal to the surface. As the yaw angle goes to  $30^\circ$  and to  $60^\circ$ , the total-pressure ratios fall rapidly and, at  $\psi = 60^\circ$ , approach closely to the free-stream static-pressure curve. It is noted that this inlet at  $\psi = 60^\circ$  offers a very wide

opening to the approaching boundary layer; thus, the inlet takes in a proportionately larger quantity of low-energy boundary-layer air. In addition, there is the simple effect of increased turning required because of yaw. These results suggest that for highest total-pressure recovery the yaw angle should be maintained as low as possible. This condition is increasingly important as the mass-flow ratio or Mach number is increased.

Effect of size of circular thin-plate inlets.- Three circular thin-plate inlets,  $t = 1/16$  inch, having diameters of 0.25, 0.375, and 0.50 inch were tested to determine the effect of the ratio of inlet diameter to boundary-layer thickness. (See fig. 8(d).) The variation of boundary-layer thickness with Mach number provided an overall range of  $D/\delta$  from 1.67 to 4.35. The total-pressure recovery for the zero mass-flow (vent) condition agrees well with the stream static-pressure curve up to  $M = 1.0$ . Above  $M = 1.0$ , however, expansions into the opening together with a shock against the downstream face of the inlet cause a slight pressure rise. At the two higher mass-flow ratios for which data are shown,  $\frac{m_i}{m_0} = 0.3$  and  $0.5$ , the pressure recovery falls to values considerably below the stream static pressure. Since the effect of the change in  $L/D$  (0.125 to 0.25) of these inlets is insignificant (see fig. 8(a)), it must be concluded that within this range of  $D/\delta$  there is little or no effect of boundary-layer thickness on the recovery of thin-plate inlets. This conclusion is in agreement with conclusions 4 and 5 of reference 3.

#### Flush Rectangular Inlets

Effect of  $\theta$ .- The pressure recovery characteristics of several rectangular inlets of width-depth ratio 4 followed by a constant-cross-section duct ( $L/D = 5$ ) are presented as figure 8(e). These inlets had a depth of 0.1875 inch which is 1.44 times the boundary-layer thickness at a Mach number of 1.0. At  $\frac{m_i}{m_0} = 0$ , the high-angle ( $30^\circ < \theta < 90^\circ$ ) rectangular inlets also have pressure recoveries closely approaching the stream static pressure up to  $M = 1.0$ . The  $\theta = 15^\circ$  inlet, when operating as a vent, however, has a recovery about 6 percent greater than the other inlets for  $M \leq 1.0$ . At supersonic Mach numbers and zero mass-flow ratio, the pressure recovery of all these inlets was about equal. As the mass-flow ratio is increased to 0.3, 0.5, or 0.7, these rectangular inlets offer pressure recoveries similar to those for the circular inlets of figure 8(b). The recovery consistently decreased as  $\theta$  increased from  $15^\circ$  to  $90^\circ$ .

Effects of ramp configuration and lip radius.- The  $\theta = 15^\circ$  inlet of figure 8(e) was modified by rounding the upstream corner of the ramp

and by rounding the inlet lip (fig. 8(f)) and by reducing the ramp angle (fig. 8(g)). It is observed in figure 8(f) that the initial straight-ramp, sharp-lip configuration had slightly less recovery than the modified configurations throughout the Mach number range for all mass-flow ratios. The 3-inch radius on the inlet ramp increased the recovery above that of the original 15° ramp configuration. No further improvement was noted for the  $4\frac{1}{2}$ -inch-ramp radius with either a sharp or rounded upper lip. Although none of these modifications resulted in marked improvements in the total-pressure recovery, the inlet-ramp radius was, effectively, a continuation of the previously discussed (figs. 8(a) and 8(e)) systematic reductions in inclination of the inlet axis. A more effective change was that of reducing the ramp approach to the inlet to 7°. This reduced-ramp angle provided increases in total-pressure recovery throughout the Mach number range but was most effective for  $M > 1.0$ . (See fig. 8(g).) It appears that, although sharp bends into the inlet should be avoided, a low angle of the entrance ramp is the primary consideration. This effect has been observed previously in investigations of submerged entrances. (See ref. 6.)

Although divergence of the ramp is not strictly a variation of inlet width-depth ratio, its effects are similar to those of width-depth ratio variation since ramp divergence also affects the boundary layer which is allowed to enter the inlet. The divergence and ramp angle for the inlet discussed here (see fig. 2(b)) is the same as the one used in reference 6. The diverging ramp inlet (fig. 8(g)) offers pressure recoveries higher than any of the other flush-type inlets tested at mass-flow ratios less than or equal to 0.5. However, for mass-flow ratios of 0.7 or greater, the 7° inclined inlet with straight-wall ramp offered higher pressure recoveries.

Effect of width-depth ratio.- Performance curves for several inlets with 15° inclination but varying width-depth ratio are presented in figure 8(h). No great advantage appears to lie in any of the configurations although the lower width-depth ratio inlets (1 and 1/4) led to slightly higher total-pressure recoveries and mass-flow ratios than the inlet with a width-depth ratio of 4 especially for  $M > 0.9$ . A study of figures 7(e) and 7(g) reveals that the inlets with lower width-depth ratios choke at higher mass-flow ratios than the width-depth-ratio-4 inlet and that in this range the total-pressure recovery is generally rising with mass-flow ratio. If there were no cross flow, decreasing the width-depth ratio would require that less low-energy boundary-layer air and more high-energy air from the free stream would enter the inlet. In this way, both the mass-flow ratio and the total-pressure recovery would be increased, as can be computed from the curves of reference 4. These increases, however, failed to materialize in the measured inlet performance partly because of cross flow over the edges of the inlet and partly because of the adverse effects of low aspect ratio on the performance of a duct bend.

In an attempt to control boundary-layer cross flow into the inlet, the aspect-ratio-1/4 inlet was equipped with fences which were especially effective in increasing the maximum mass-flow and total-pressure ratios (fig. 7(g)) although the total-pressure recovery at lower mass-flow ratios shown in figure 8(h) was not improved.

The flush circular inlet data (for  $\psi = 0^\circ$  and  $\theta = 15^\circ$ ) have been replotted in figure 8(h). Although the cross-sectional area of these inlets is different from that of the rectangular inlets, the width-depth ratio is regarded as unity and it may be compared with the rectangular inlets on this basis. At mass-flow ratios less than or equal to 0.5, the circular inlet performance is equal to that of the rectangular inlets with low width-depth ratios. At  $\frac{m_1}{m_0} = 0.7$ , however, the circular inlet pressure recovery falls 2 to 3 percent below that of the rectangular inlets for Mach numbers greater than about 0.7.

#### Circular Scoops

A circular scoop inlet constructed so that the inner edge of the lip is flush with the surface of the tunnel wall was tested at yaw angles of  $0^\circ$ ,  $30^\circ$ , and  $60^\circ$ . The inlet diameter is 0.375 inch; thus,  $D/\delta = 2.88$  at  $M = 1.0$ . Results are presented in figure 8(i). It is immediately observed that the total-pressure recovery for  $0^\circ$  yaw is much higher than that for the best of the flush inlets. Total-pressure ratios remained above 0.90 for all test Mach numbers for  $m_1/m_0$  up to 0.7 and up to the choked condition for most Mach numbers. (See fig. 7(h).) Yawing the inlet caused marked reductions in total-pressure recovery for values of  $\psi$  approaching  $60^\circ$  where, for  $m_1/m_0 = 0.5$ , the scoop inlet pressure recovery was less than that for the flush circular inlet ( $\theta = 15^\circ$ ) at  $\psi = 60^\circ$ . For the zero mass-flow condition, it was found that the slope of the recovery curve for the scoop inlet closely approximates that for the total-pressure tubes reported in reference 7. The magnitudes of the pressures are not comparable with those of reference 7, however, because of the boundary layer in which the inlet operated.

#### Ramp Static-Pressure Distributions

Four of the inlets previously discussed were equipped with static-pressure orifices down the center of the ramp in an effort to obtain a better understanding of the flow as it approaches the inlet.

Rectangular inlet;  $\theta = 15^\circ$ ; width-depth ratio of 4. - The static-pressure distributions for the rectangular inlet with a sharp lip and a

$4\frac{1}{2}$ -inch radius on the ramp are presented as figure 9(a). A small tick on the ordinate indicates stream static pressure. The pressure on the upstream end of the ramp decreases slightly below the stream static pressure as the air is accelerated locally in turning from the surface onto the ramp. At low mass-flow ratios this local acceleration is immediately followed by a pressure rise ahead of the inlet lips followed by nearly constant or gradually increasing pressure through the inlet duct. As the mass-flow ratio increases, the local accelerations on the inlet ramp become stronger and are followed by a compression that was also observed at low mass-flow ratios. For  $M_\infty > 1.0$ , none of the pressures on the ramp were as low as the theoretical values corresponding to the turning angle of the ramp. This condition is probably due to the boundary-layer flow and possible separation from the ramp leading edge. For each Mach number, the pressures indicated a net turn of from  $5^\circ$  to  $7^\circ$ .

For the highest mass-flow ratios, the static pressure inside the inlet duct decreased at  $M_\infty \approx 0.9$  but remained nearly constant or continued to rise for  $M_\infty > 1.0$ . This result is readily explained in terms of the static pressure necessary for choking, the total-pressure losses being assumed as not excessive. For the inlets to choke at subsonic speeds, the static pressure must necessarily decrease; however, at supersonic speeds, the Mach number at choke is less than the free-stream Mach number and choking incurs a pressure rise. Since the inlet lip angle is greater than the maximum for which attached shocks can occur at these Mach numbers, it is obvious that a strong shock remains upstream of station 0 at all supersonic Mach numbers and the flow downstream of station 0 must remain subsonic for all flow conditions. Rounding the lip of this inlet resulted in the static-pressure distributions of figure 9(b). These distributions are notably similar to those of figure 9(a) and no gross effects due to lip radius are observed.

Rectangular inlet, ramp angle  $7^\circ$ .—The sharp-lip rectangular inlet,  $\theta = 15^\circ$ , with a straight-sided ramp of  $7^\circ$  produced the ramp static-pressure distributions of figure 9(c). For low Mach numbers,  $M_\infty \approx 1.0$ , the upstream end of the ramp behaves much the same way as a subsonic diffuser and causes the static pressure to rise for all mass-flow ratios. The maximum pressure is generally reached at the inlet lip and the flow through the inlet duct follows the same pattern as was observed in figure 9(a). At the highest mass-flow ratio, there is an abrupt pressure drop at station 0. A similar but somewhat less abrupt pressure drop is observed for the inlets of figures 9(a) and 9(b). It may therefore be surmised that, for the inlets without ramps (that is,  $\phi$  and  $\theta$  equal), this initial pressure reduction at, or slightly inside, the lip stems from local accelerations on the inner surface of the lip. For inlets with  $\phi < \theta$ , the pressure drop at the lips would result from a combination

of local acceleration on the inner surface of the lip and at the ramp-throat juncture. For  $M_{\infty} > 1.0$ , the flow at the upstream end of the ramp experiences a pressure reduction as a result of supersonic acceleration but almost immediately begins a gradual recompression which continues up to the face of the inlet. A gradual compression of this type would be expected to offer a higher total-pressure recovery than the strong shocks of figures 9(a) and 9(b). The internal flow is very similar to that at  $M_{\infty} \lesssim 1.0$  with the exception that the sharp pressure reduction at the lips does not occur.

Diverging ramp inlet.- The static-pressure distributions for the diverging ramp inlet (fig. 9(d)) indicate an acceleration in the upstream part of the ramp for all Mach numbers at all except the lowest mass-flow ratios. After this acceleration there is a pressure rise which occurs much more abruptly than that observed for the straight-walled ramp. The upstream ramp acceleration at  $M_{\infty} \lesssim 1.0$  must represent a supersonic expansion and Mach numbers up to 1.18 and 1.5 are indicated for free-stream Mach numbers of 1.0 and 1.3, respectively. The very abrupt pressure rise occurring up to 1/2 inch ahead of the inlet lips obviously is a strong shock and is similar to that observed for the inlets of figures 9(a) and 9(b). A shock with probable separation was observed in this region for a similar inlet in reference 8. The losses in a strong shock in this region are much less desirable than the more gradual pressure rise noted for the inlet with straight-walled ramp. The large amount of supersonic acceleration on the diverging wall ramp and the ensuing shock at relatively high Mach numbers are the cause of high losses which occurred with this inlet at the higher mass-flow ratios.

#### CONCLUSIONS

A transonic investigation of the pressure recovery and mass-flow characteristics of several flush type and one scoop-type auxiliary inlets immersed in relatively thick boundary layers has permitted the formulation of the following conclusions:

1. Best pressure recovery and highest mass-flow rates were obtained with a scoop inlet; inclined inlets wherein the inlet axis and/or ramp is at a very low angle with respect to the surface were the best of the flush installations tested.
2. For flush inlets, if the inlet is small and operates at the high mass-flow ratios, best total-pressure recovery was obtained when a low width-depth ratio and parallel fences were used to restrict the cross flows.

~~CONFIDENTIAL~~

3. The diverging ramp inlet ( $\phi = 7^\circ$ ) was inferior to the parallel-sided ramp ( $\phi = 7^\circ$ ) at high mass-flow ratios. For low values of  $m_1/m_0$  the total-pressure recovery can be improved by using the NACA submerged inlet with diverging ramp.

4. For Mach numbers greater than 1.0, the static pressures measured along the ramp center line indicated that the diverging wall ramp caused increases in local velocities and strong shocks on the ramp.

Langley Aeronautical Laboratory,  
National Advisory Committee for Aeronautics,  
Langley Field, Va., January 30, 1956.

~~CONFIDENTIAL~~

## REFERENCES

1. Nelson, William J., and Cabbage, James M., Jr.: Effects of Slot Size and Geometry on the Flow in Rectangular Tunnels at Mach Numbers up to 1.4. NACA RM L53B16, 1953.
2. Rogallo, F. M.: Internal-Flow Systems for Aircraft. NACA Rep. 713, 1941.
3. Chew, William L.: Cross-Flow Calibration at Transonic Speeds of Fourteen Perforated Plates With Round Holes and Airflow Parallel to the Plates. AEDC-TR-54-65 (Contract No. AF 18(600)-1233), Arnold Eng. Dev. Center, U. S. Air Force, July 1955.
4. Simon, Paul C., and Kowalski, Kenneth L.: Charts of Boundary-Layer Mass Flow and Momentum for Inlet Performance Analysis - Mach Number Range, 0.2 to 5.0. NACA TN 3583, 1955.
5. Fradenburgh, Evan A., and Wyatt, DeMarquis D.: Theoretical Performance Characteristics of Sharp-Lip Inlets at Subsonic Speeds. NACA Rep. 1193, 1954. (Supersedes NACA TN 3004.)
6. Mossman, Emmet A., and Randall, Lauros M.: An Experimental Investigation of the Design Variables for NACA Submerged Duct Entrances. NACA RM A7I30, 1948.
7. Humphreys, Milton D.: Effects of Compressibility and Large Angles of Yaw on Pressure Indicated by a Total-Pressure Tube. NACA WR L-77, 1945. (Formerly NACA RB L5C30.)
8. Braden, John A., and Pierpont, P. Kenneth: Pressure and Force Characteristics at Transonic Speeds of a Submerged Divergent-Walled Air Inlet on a Body of Revolution. NACA RM L53C13, 1953.

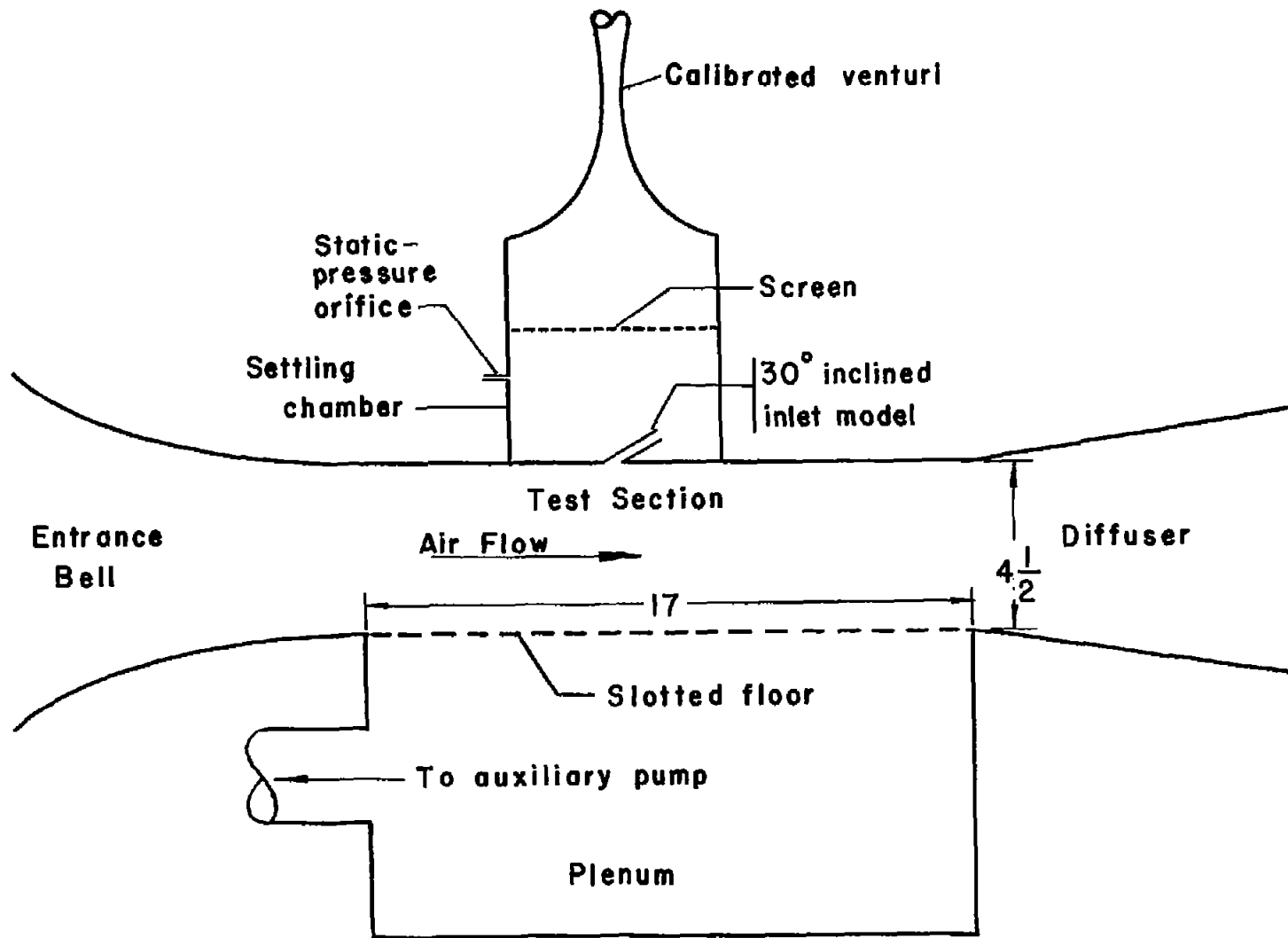
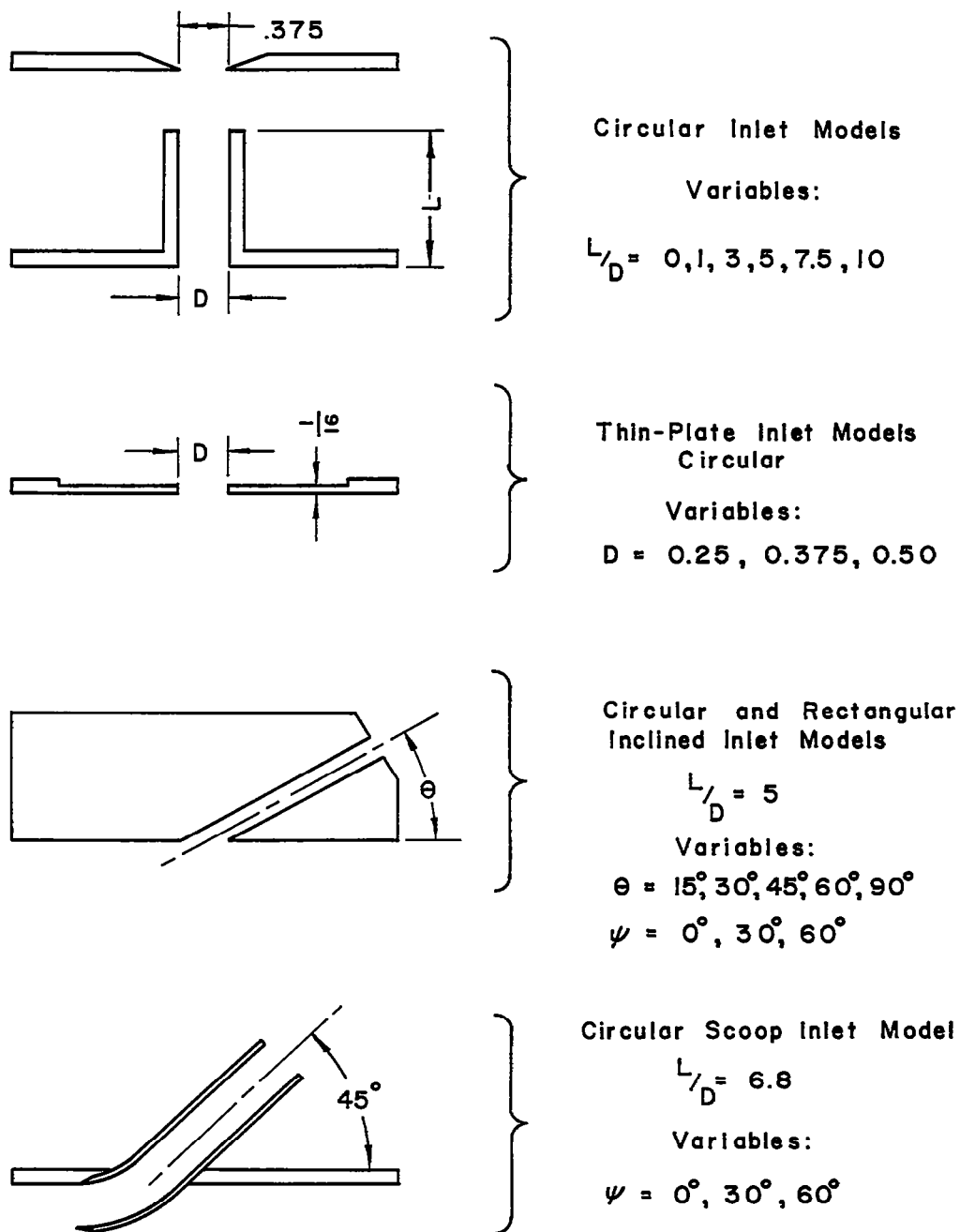
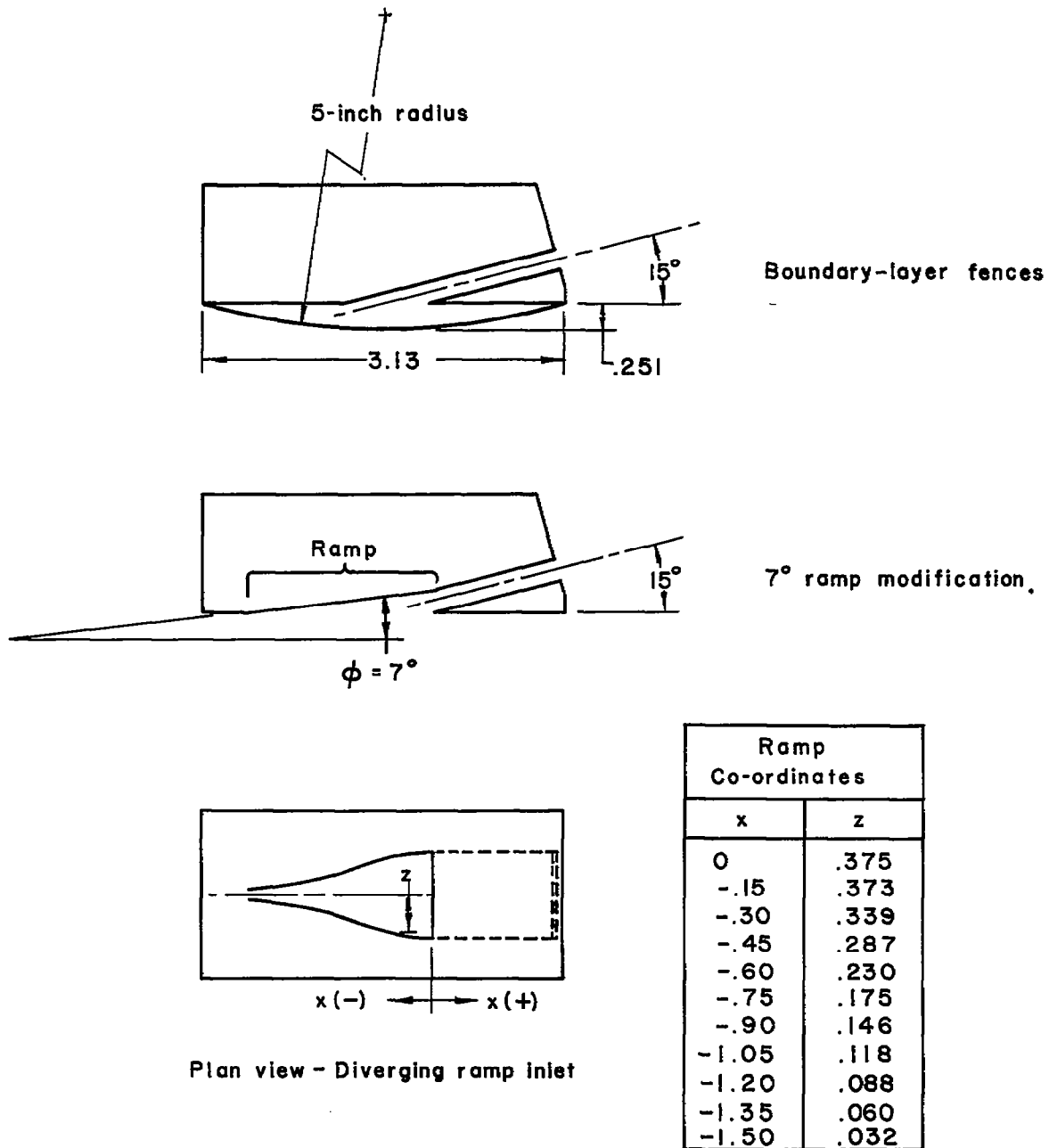


Figure 1.- Line drawing showing the general arrangement of the test setup. Linear dimensions are in inches.



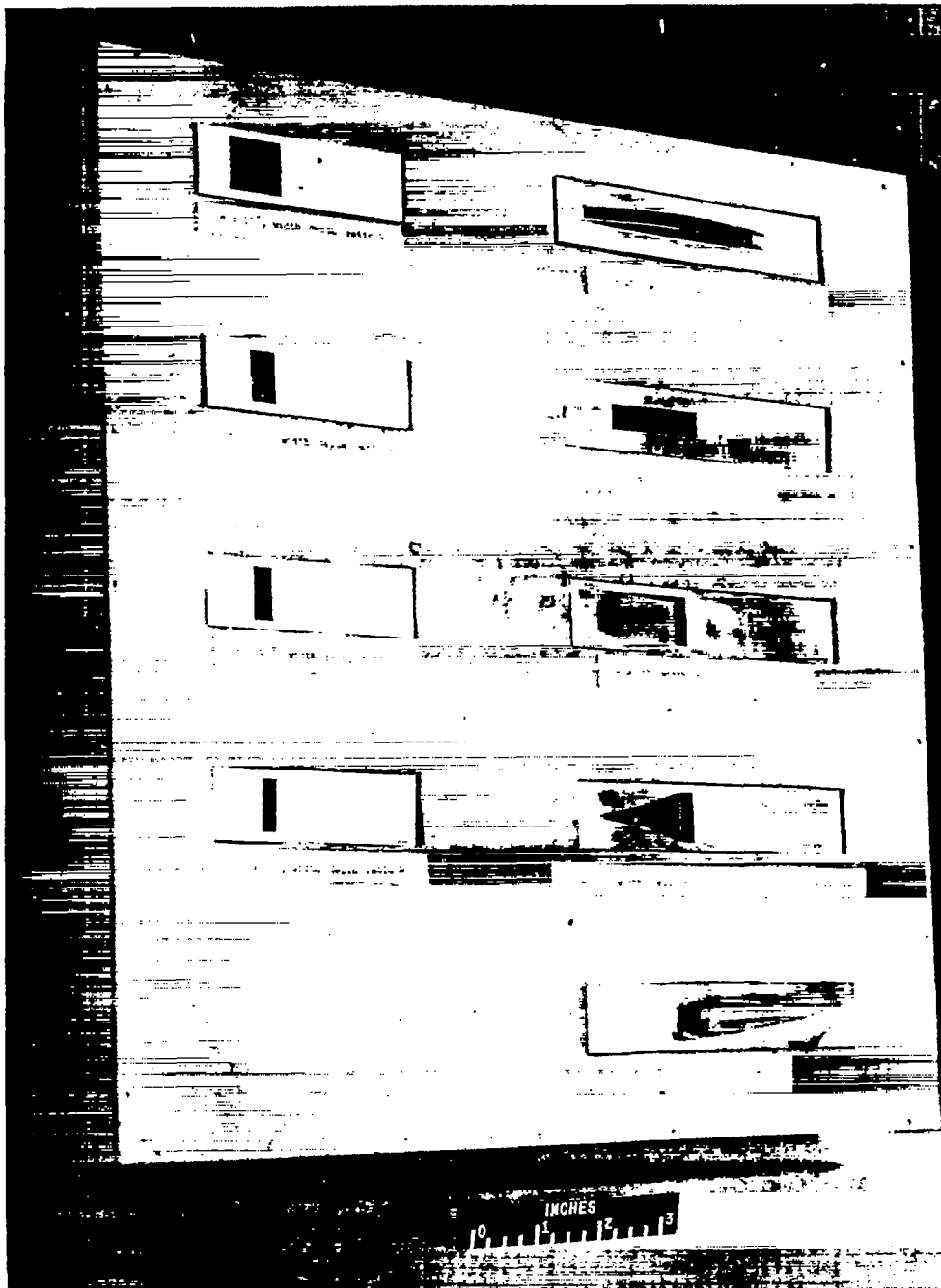
(a) Basic inlet shapes.

Figure 2.- Line drawings of the models tested.



(b) Modifications to the 15° inclined inlet.

Figure 2.- Concluded.



L-96963

Figure 3.- Photograph of the rectangular and scoop inlets.

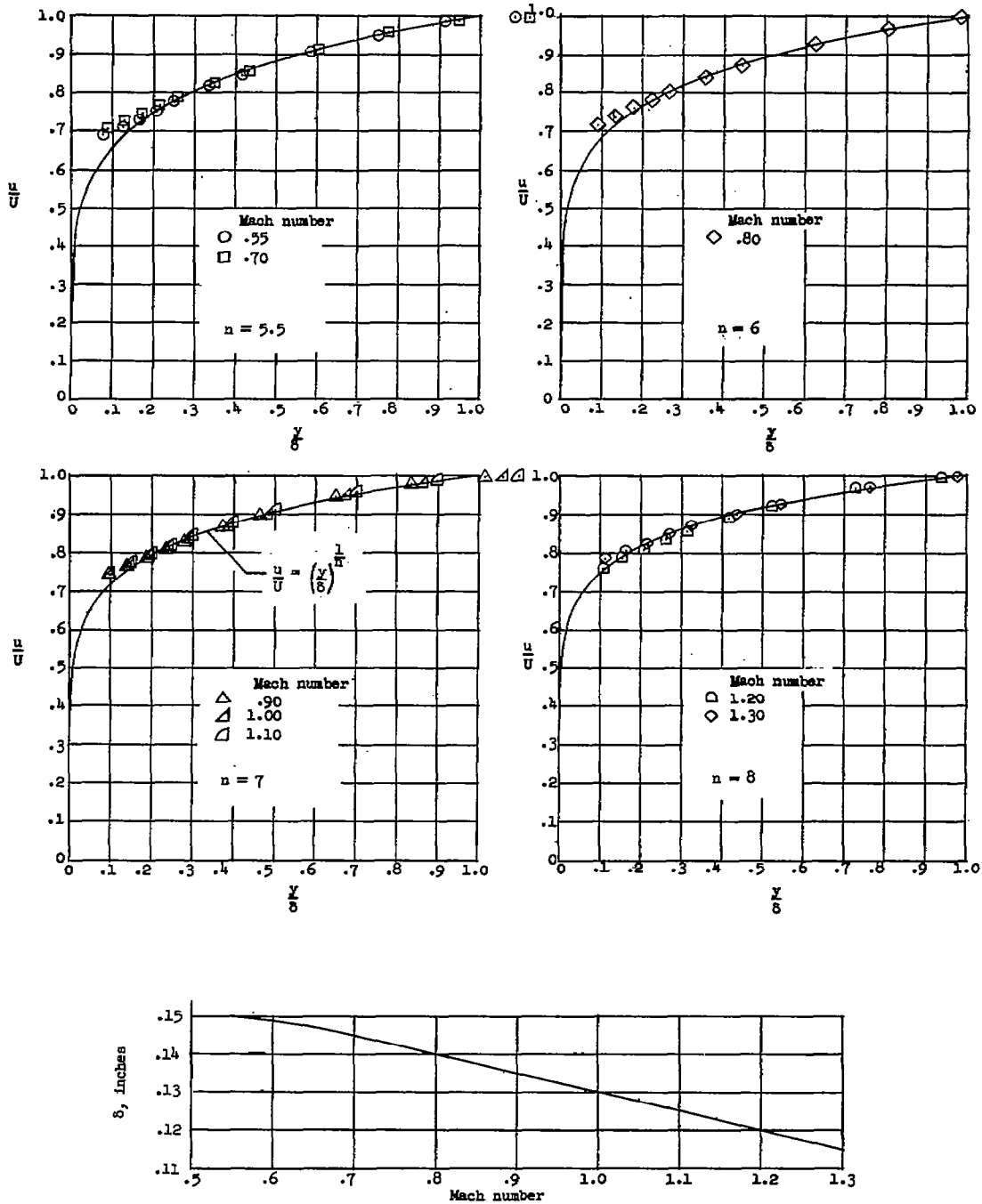
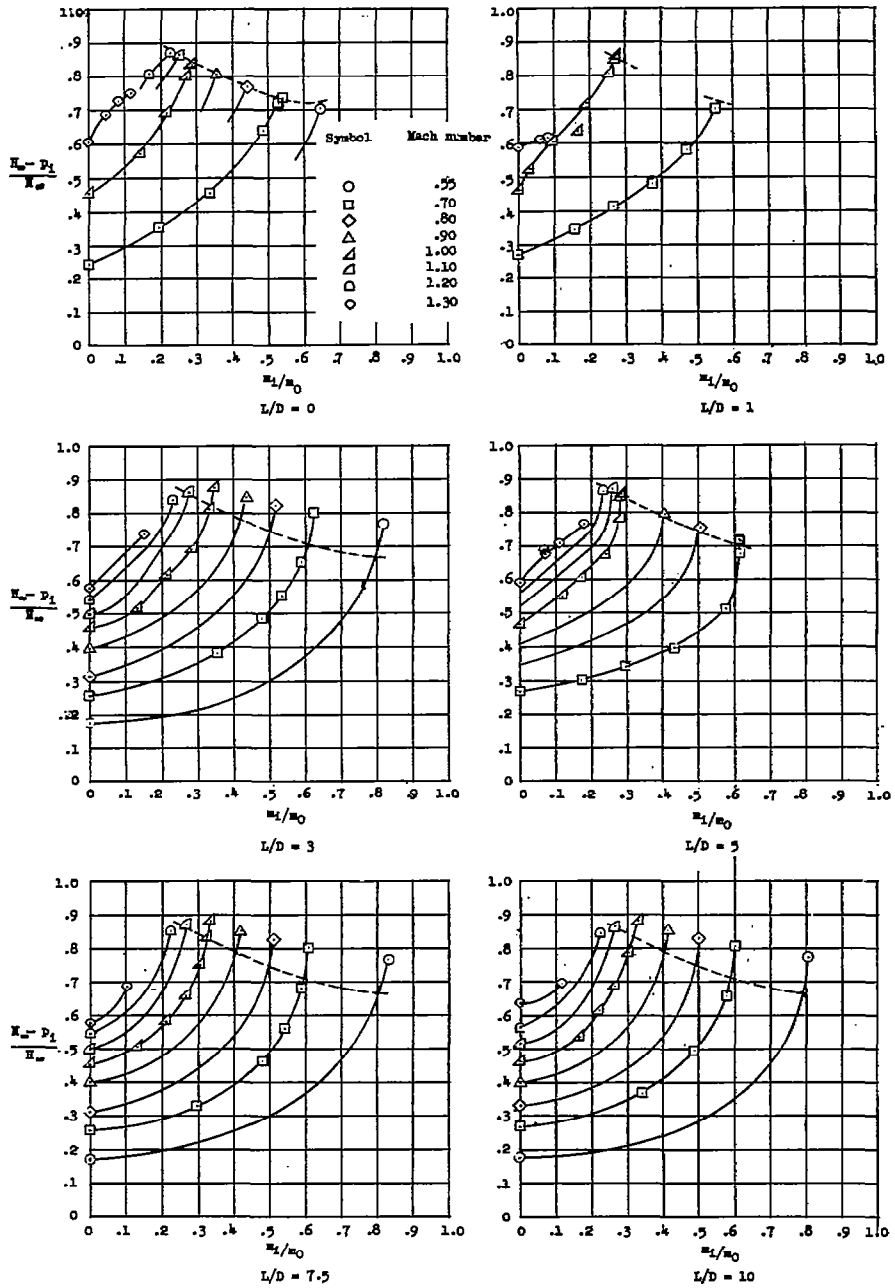
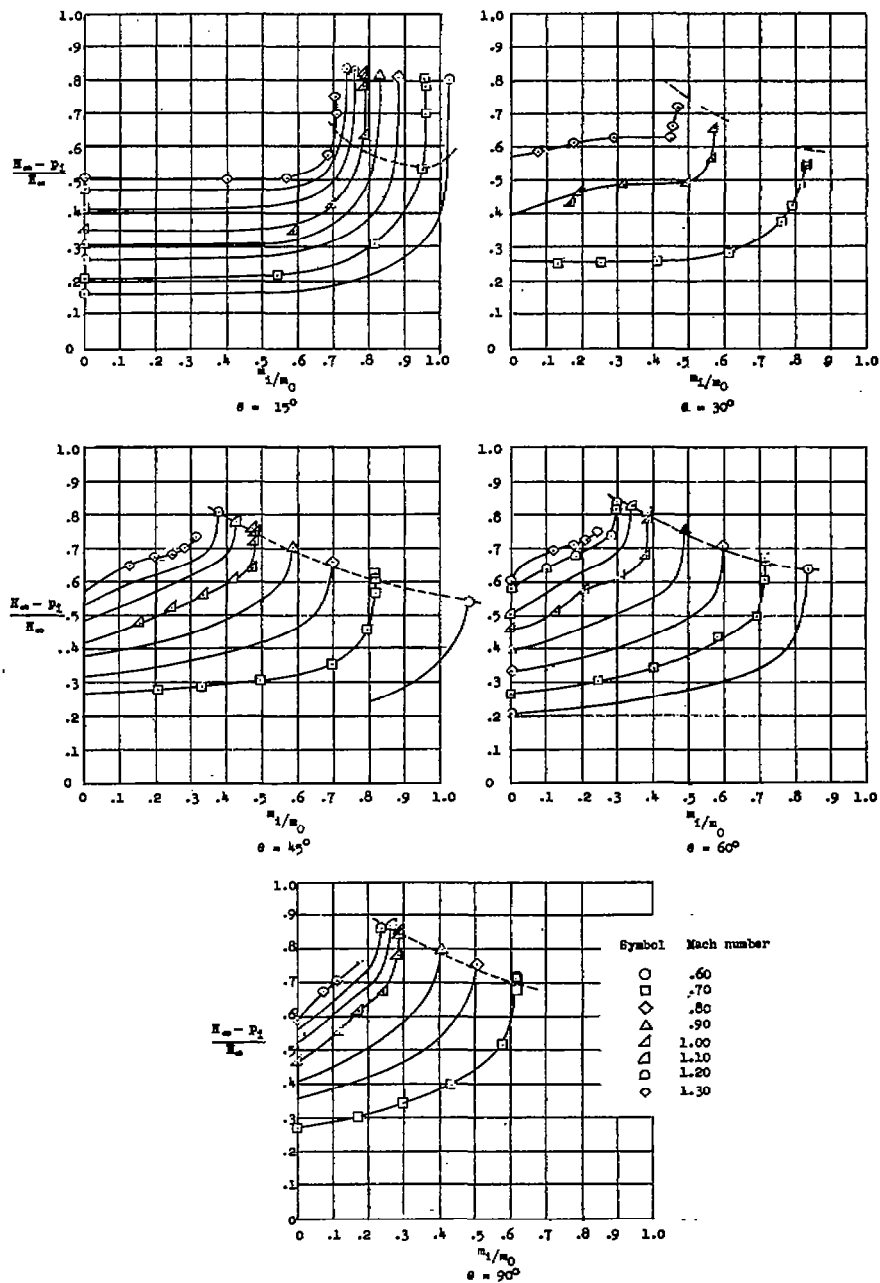


Figure 4.- Velocity distributions and boundary-layer thickness for each of the test Mach numbers.



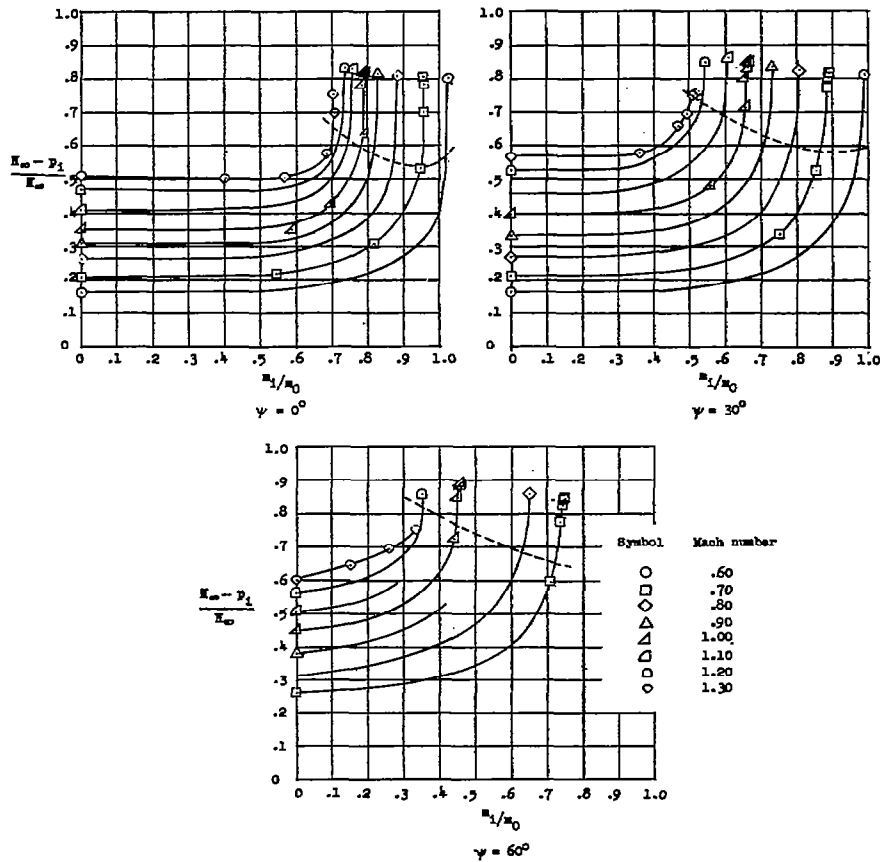
(a) Flush circular inlets; varying  $L/D$ ;  $\theta = 90^\circ$ .

Figure 5.- Variation of inlet pressure differential with mass-flow ratio.



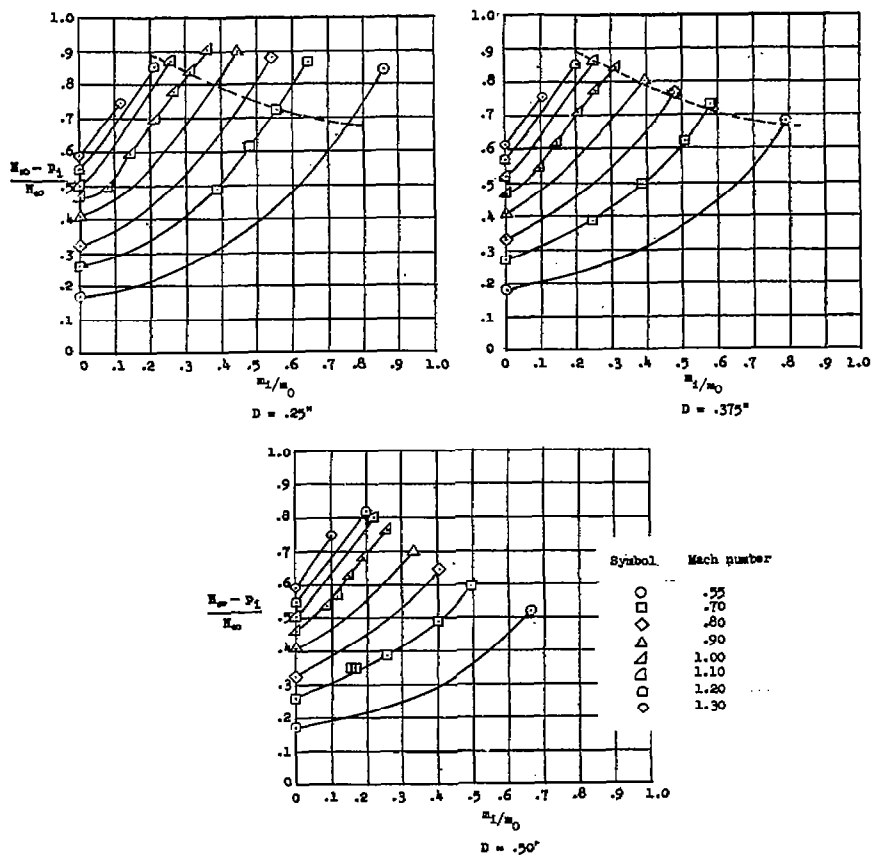
(b) Flush circular inlets; varying  $\theta$ ;  $L/D = 5$ ;  $\psi = 0^\circ$ .

Figure 5.- Continued.



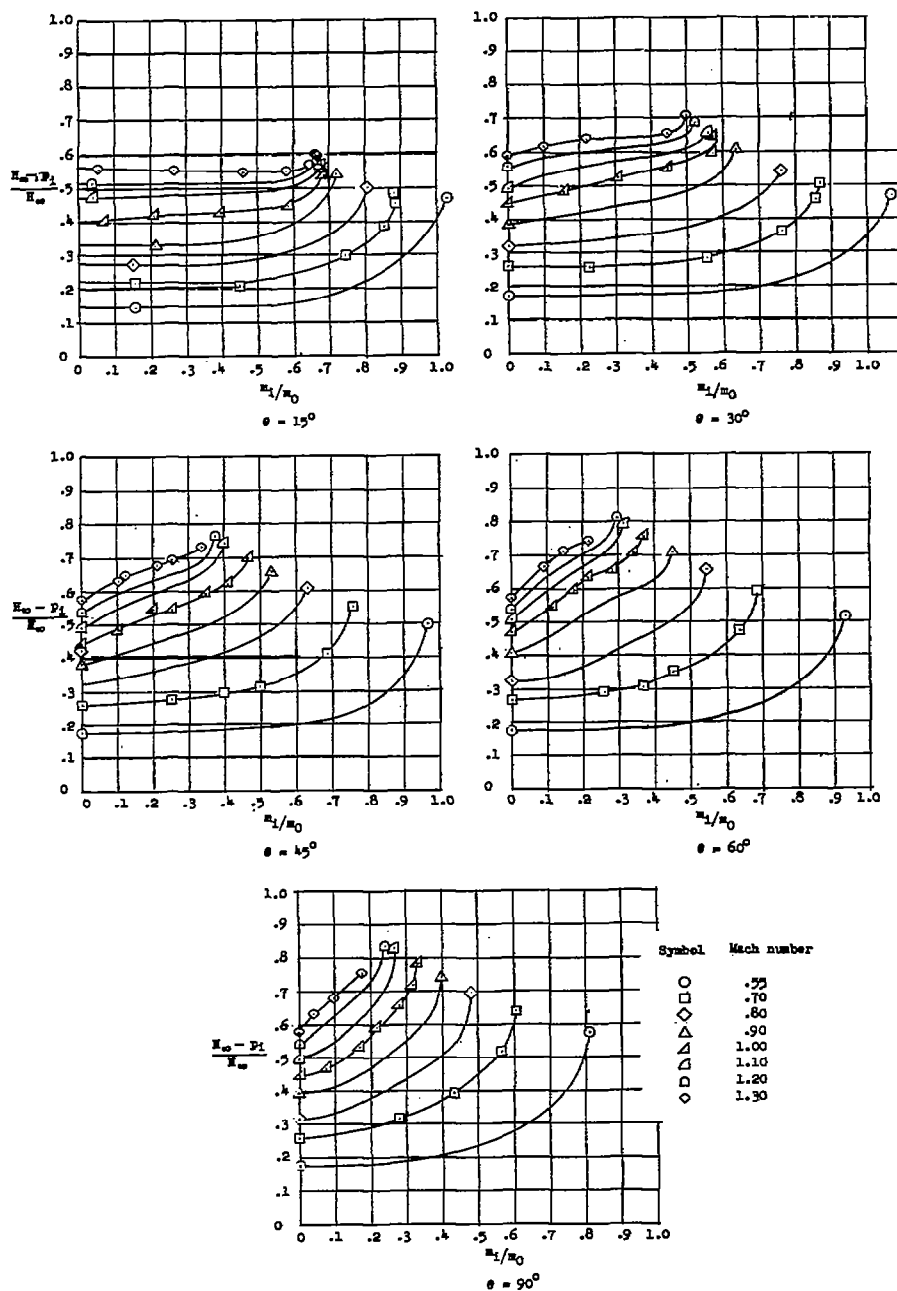
(c) Flush circular inlets; varying  $\psi$ ;  $L/D = 5$ ;  $\theta = 15^\circ$ .

Figure 5.- Continued.



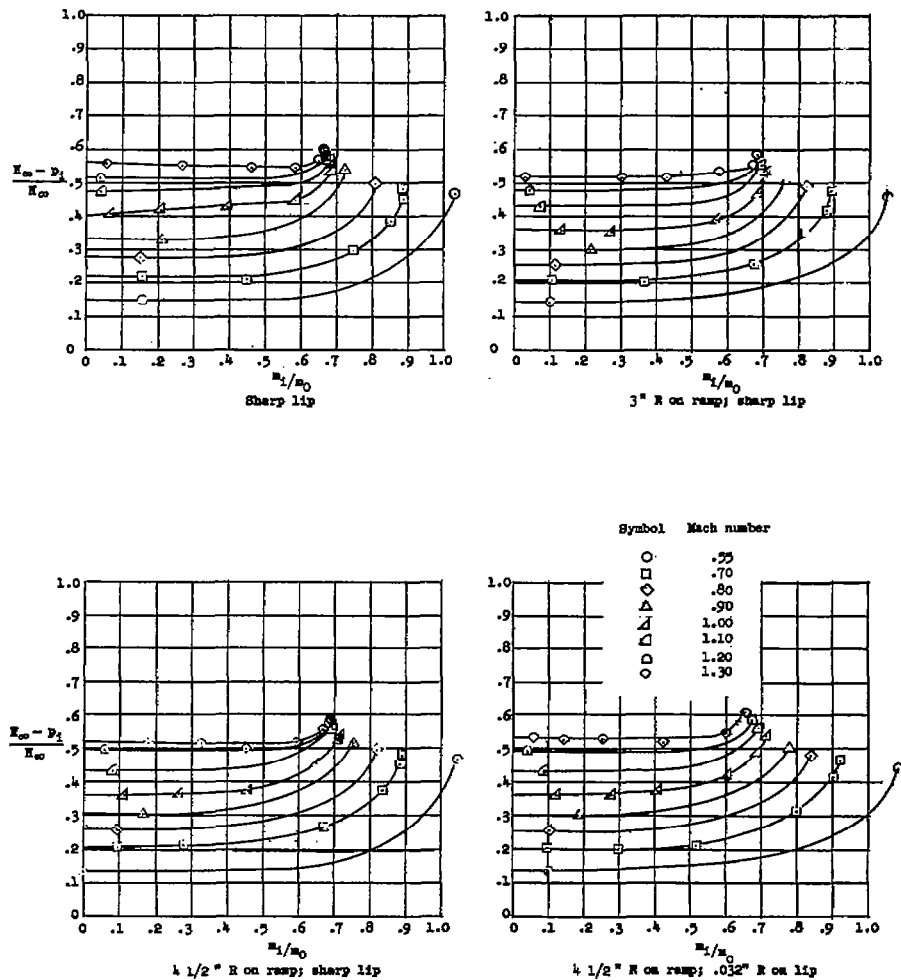
(d) Thin-plate inlets;  $t = 1/16$  inch.

Figure 5.- Continued.



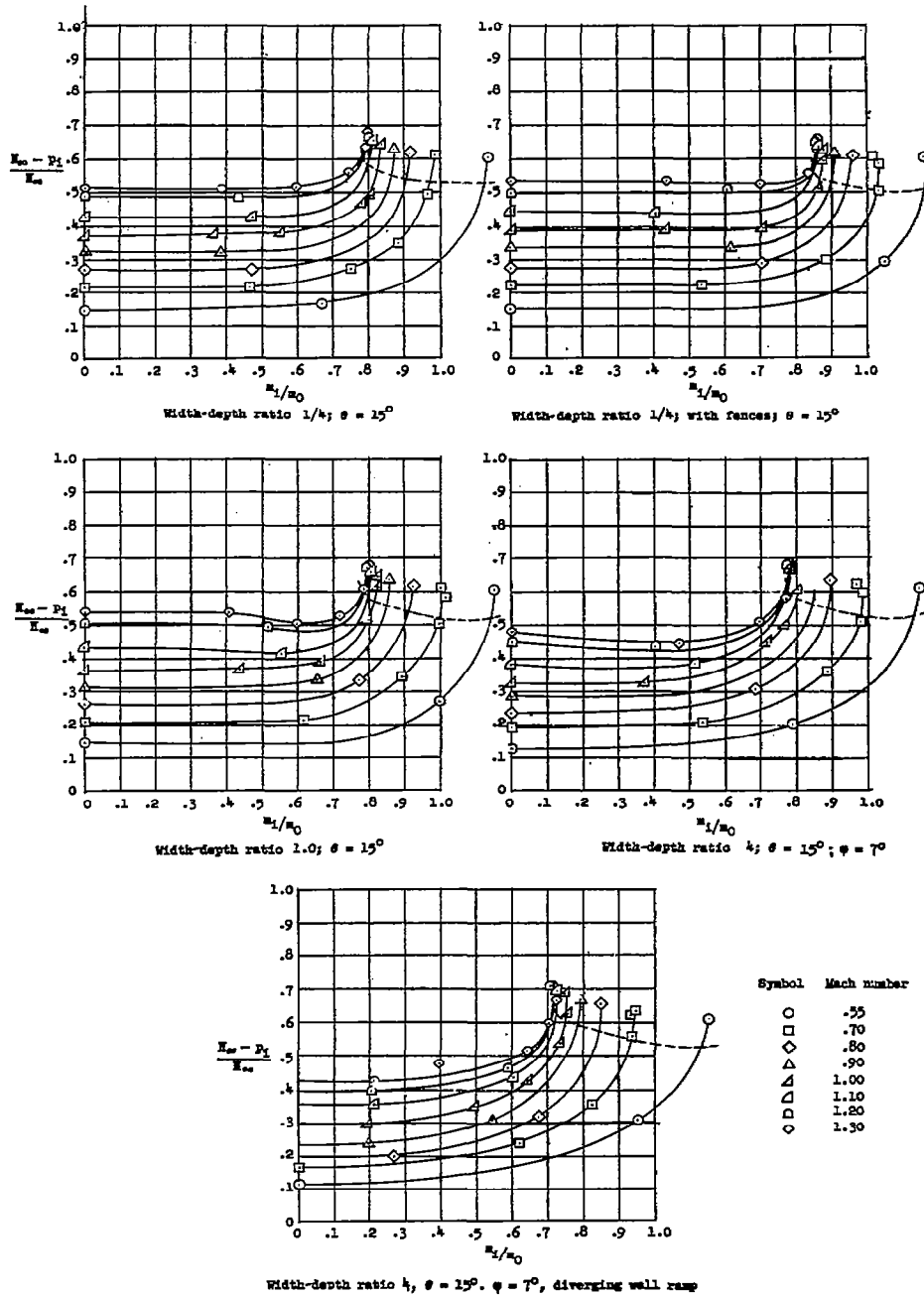
(e) Flush rectangular inlets; varying  $\theta$ ;  $L/D = 5$ ;  $\psi = 0^\circ$ ; width-depth ratio 4.

Figure 5.- Continued.



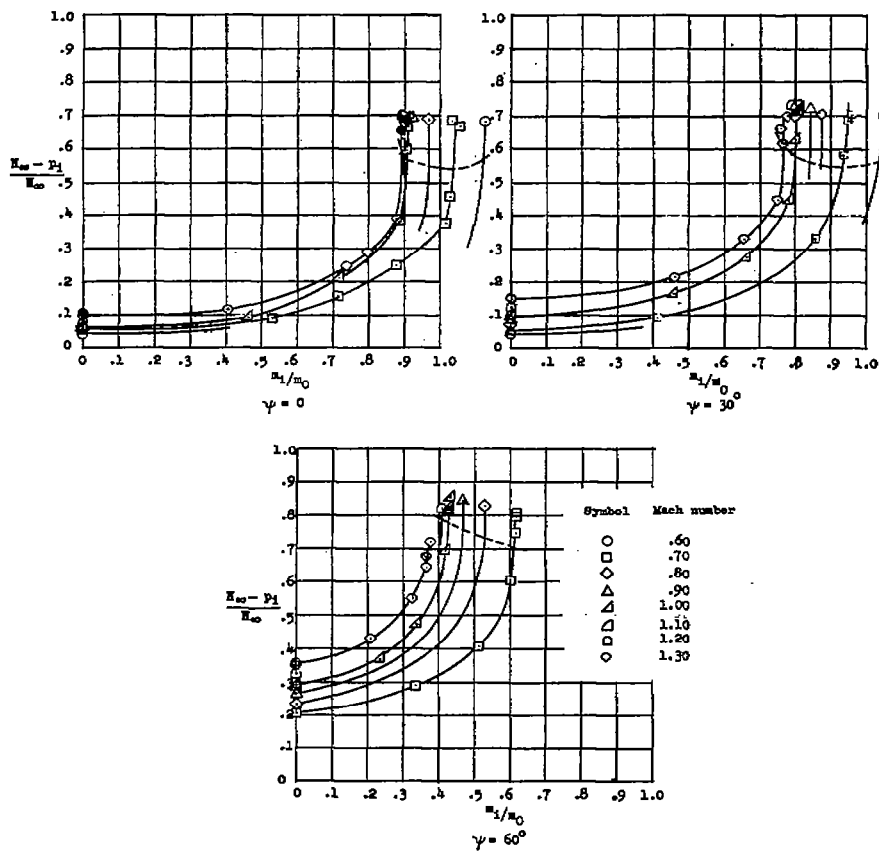
(f) Flush rectangular inlets; varying entrance geometry;  $\theta = 15^\circ$ ;  $L/D = 5$ ;  $\psi = 0^\circ$ ; width-depth ratio 4.

Figure 5.- Continued.



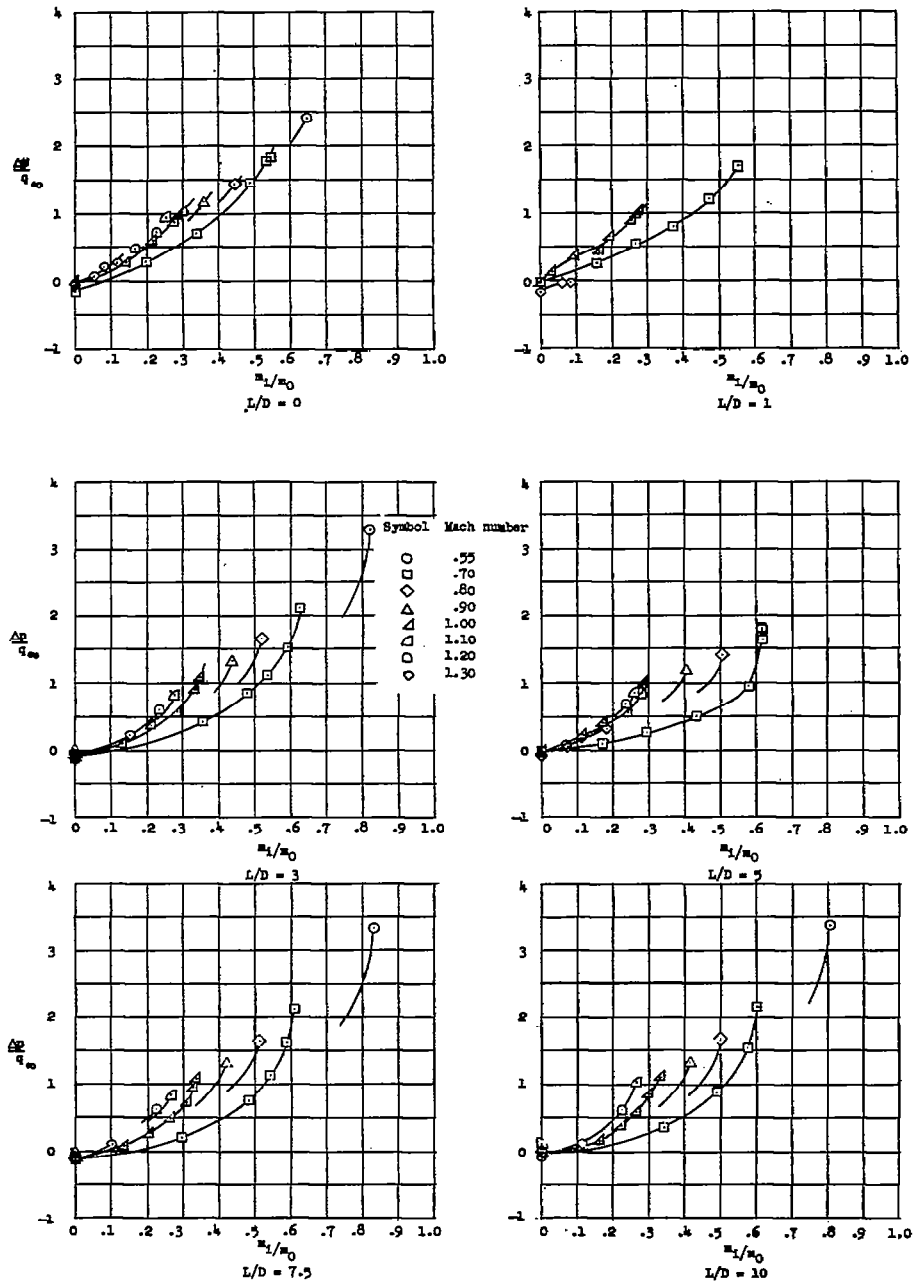
(g) Flush rectangular inlets; varying width-depth ratio and  $\phi$ ;  $L/D = 5$ ;  
 $\psi = 0$ .

Figure 5.- Continued.



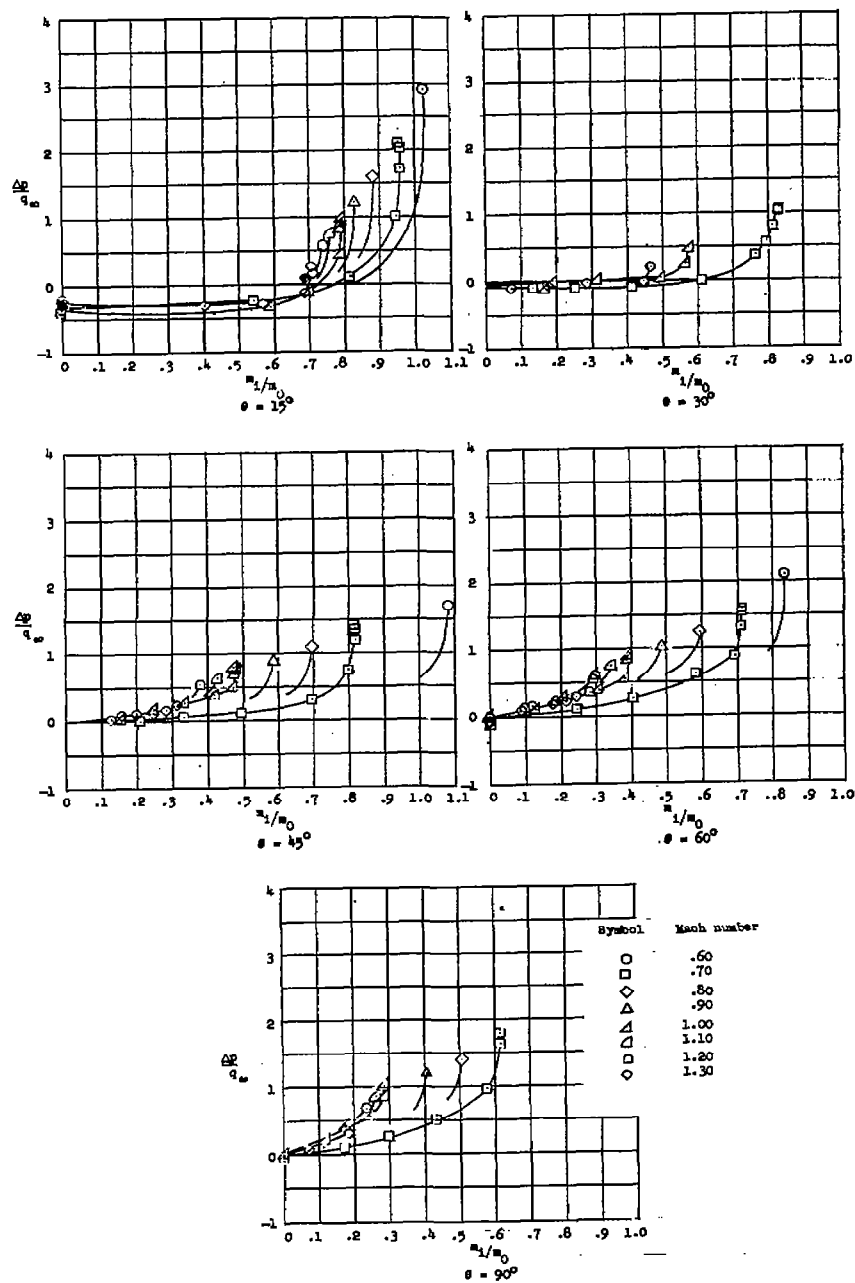
(h) Circular scoop inlets; varying  $\psi$ ;  $L/D = 6.8$ .

Figure 5.- Concluded.



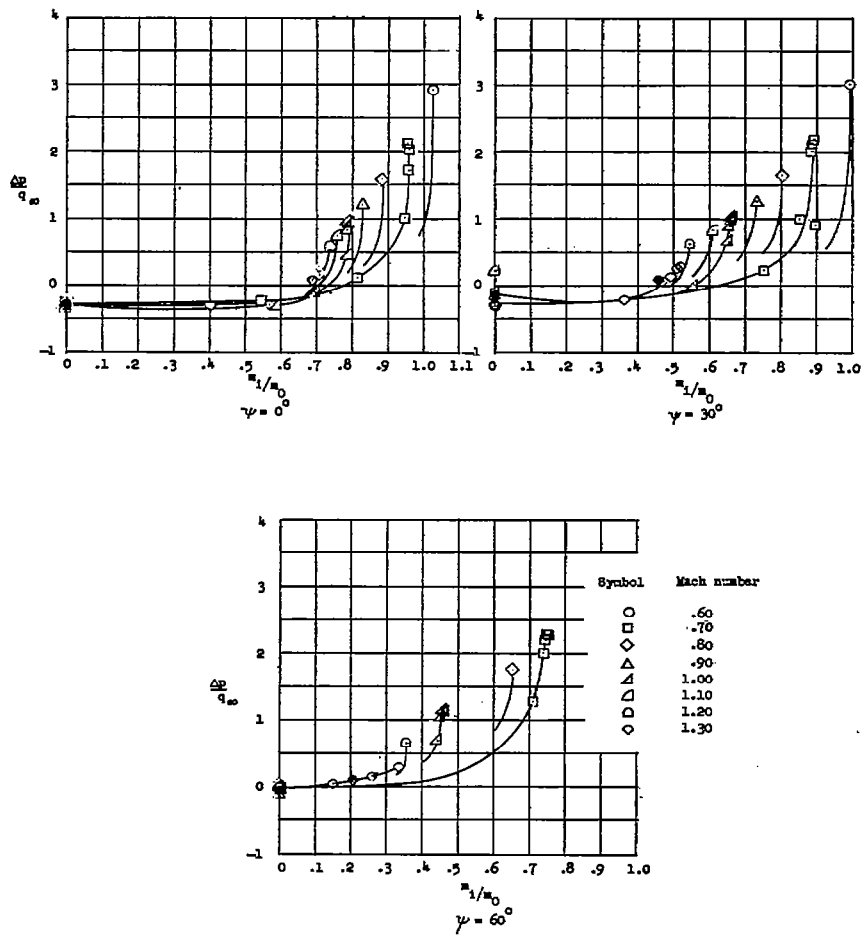
(a) Flush circular inlets; varying  $L/D$ ;  $\theta = 90^\circ$ .

Figure 6.- Variation of inlet static-pressure differential with mass-flow ratio.



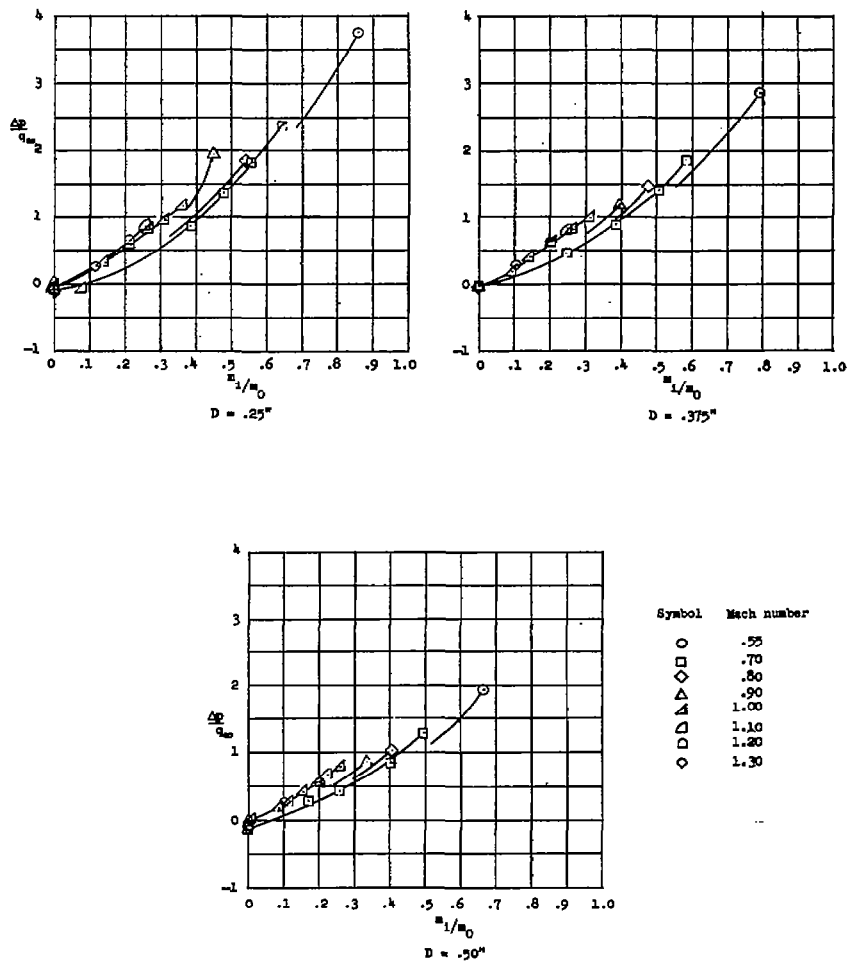
(b) Flush circular inlets; varying  $\theta$ ;  $L/D = 5$ ;  $\psi = 0^\circ$ .

Figure 6.- Continued.



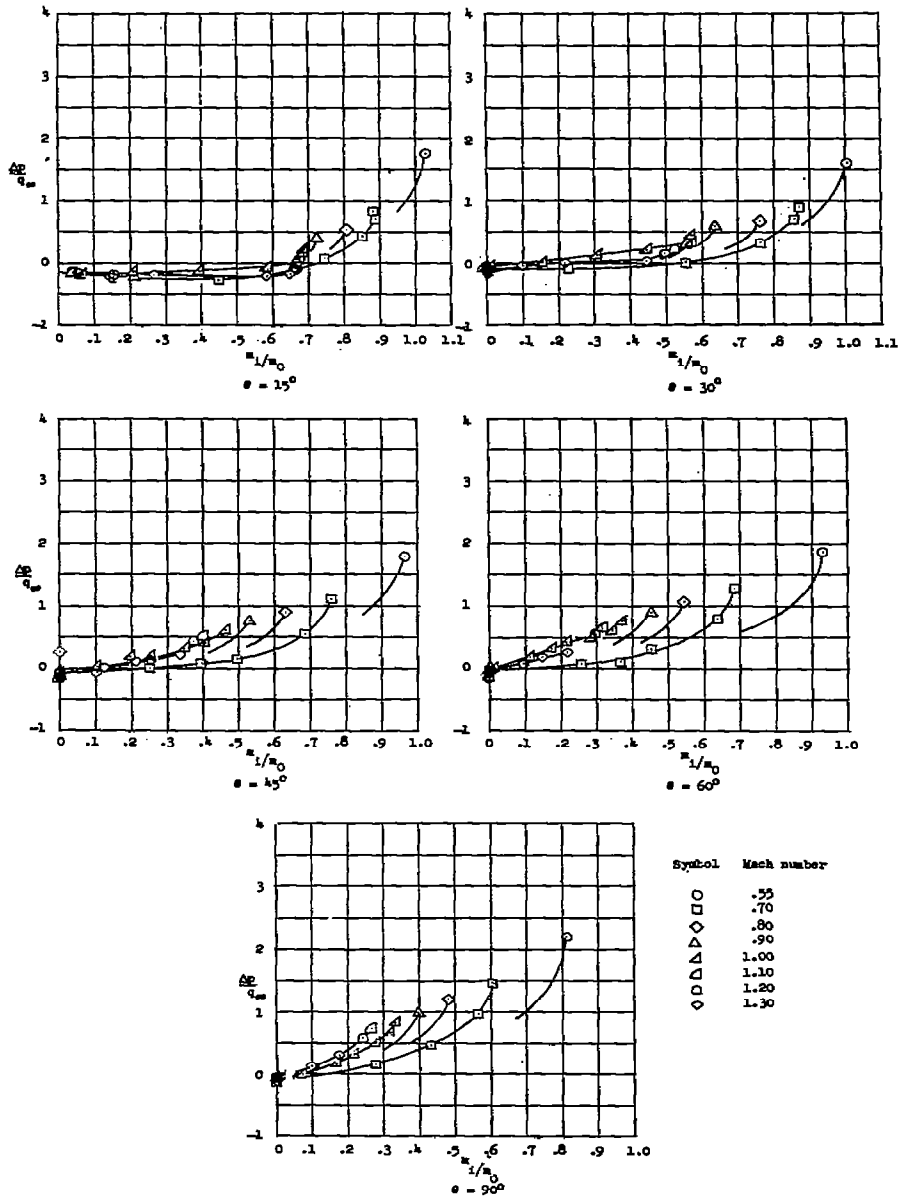
(c) Flush circular inlets; varying  $\psi$ ;  $L/D = 5$ ;  $\theta = 15^\circ$ .

Figure 6.- Continued.



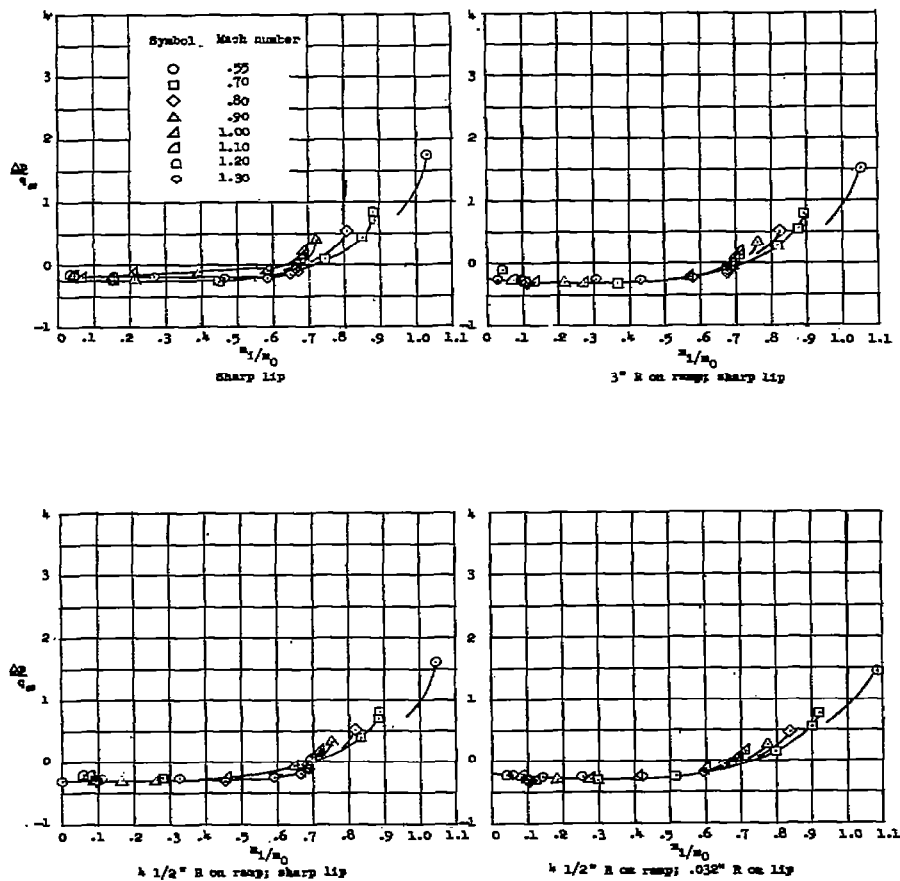
(d) Thin-plate inlets;  $t = 1/16$  inch.

Figure 6.- Continued.



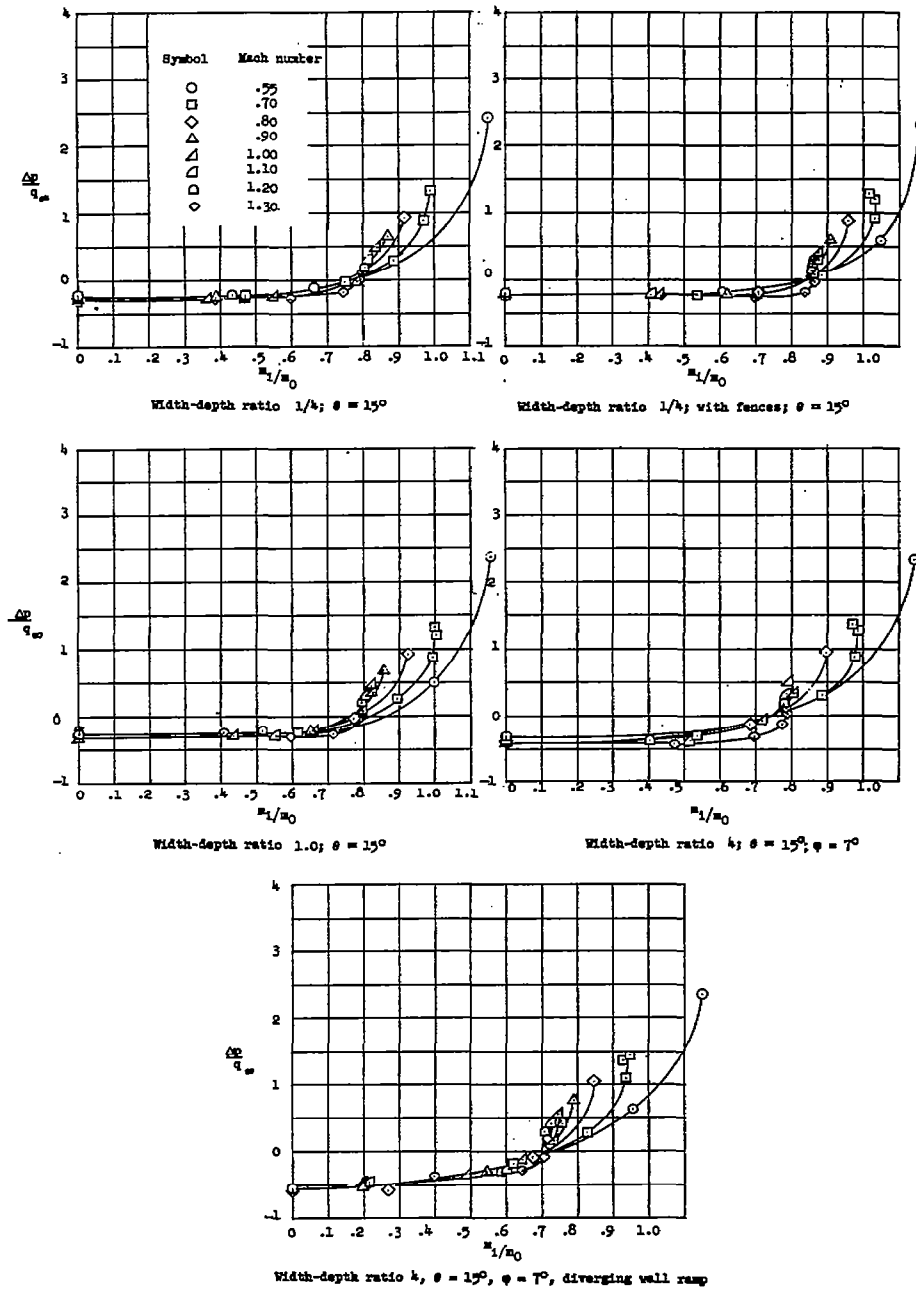
(e) Flush rectangular inlets; varying  $\theta$ ;  $L/D = 5$ ;  $\psi = 0^\circ$ ; width-depth ratio 4.

Figure 6.- Continued.



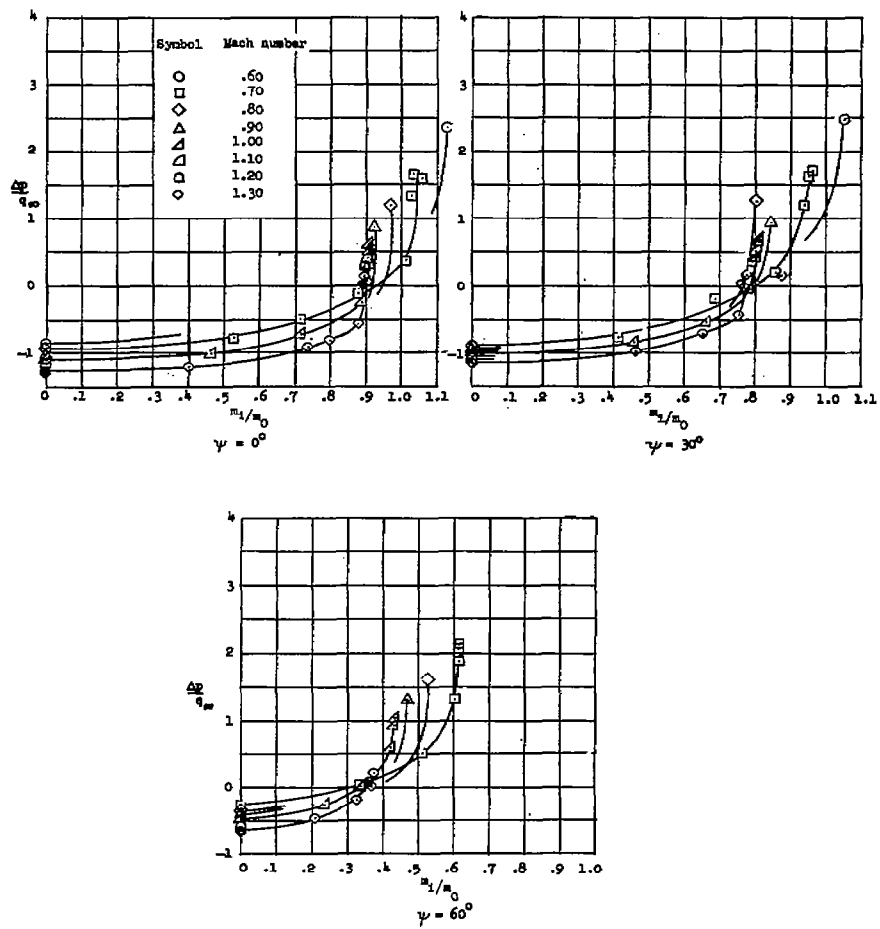
(f) Flush rectangular inlets; varying entrance geometry;  $\theta = 15^\circ$ ;  $L/D = 5$ ;  
 $\psi = 0^\circ$ ; width-depth ratio 4.

Figure 6.- Continued.



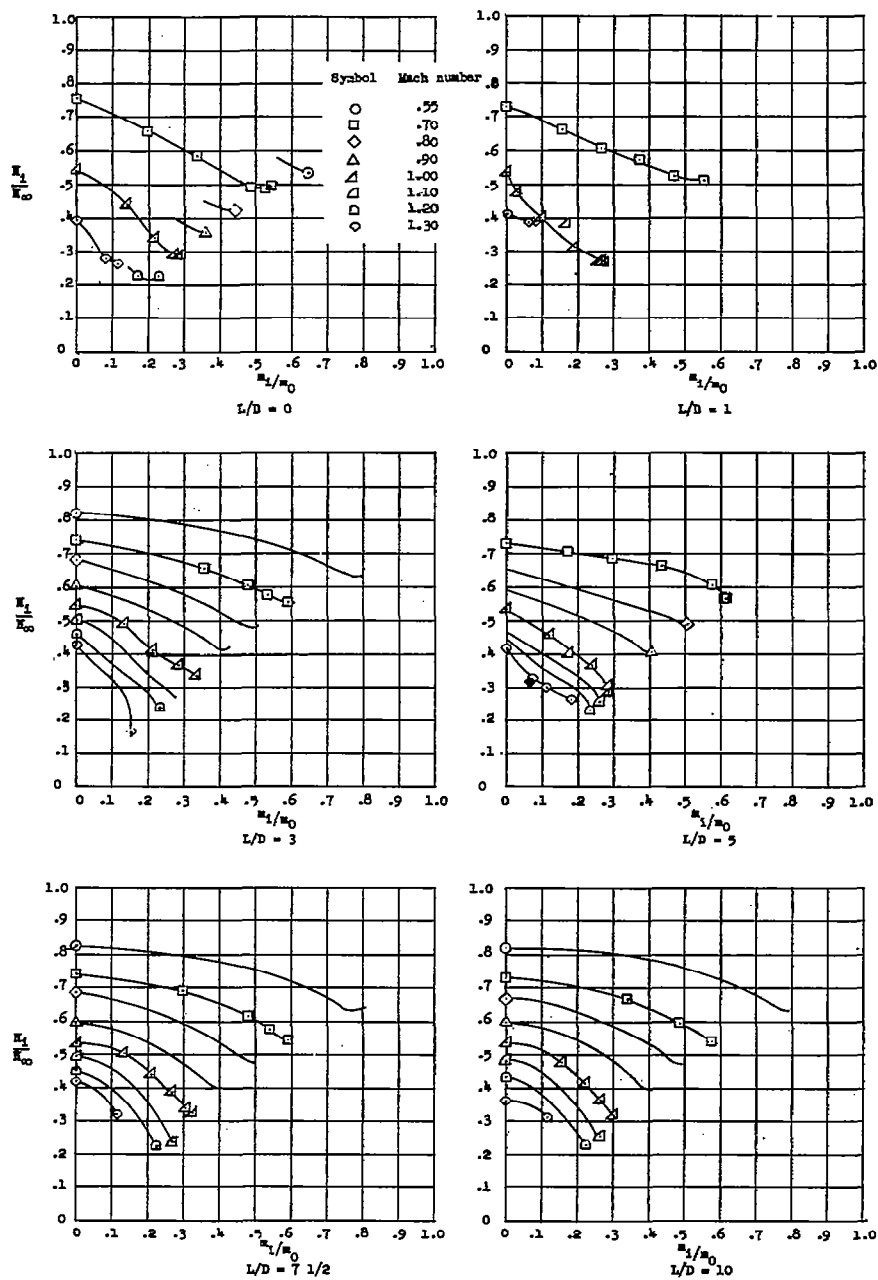
(g) Flush rectangular inlets; varying width-depth ratio and  $\varphi$ ;  $L/D = 5$ ;  
 $\psi = 0^\circ$ .

Figure 6.- Continued.



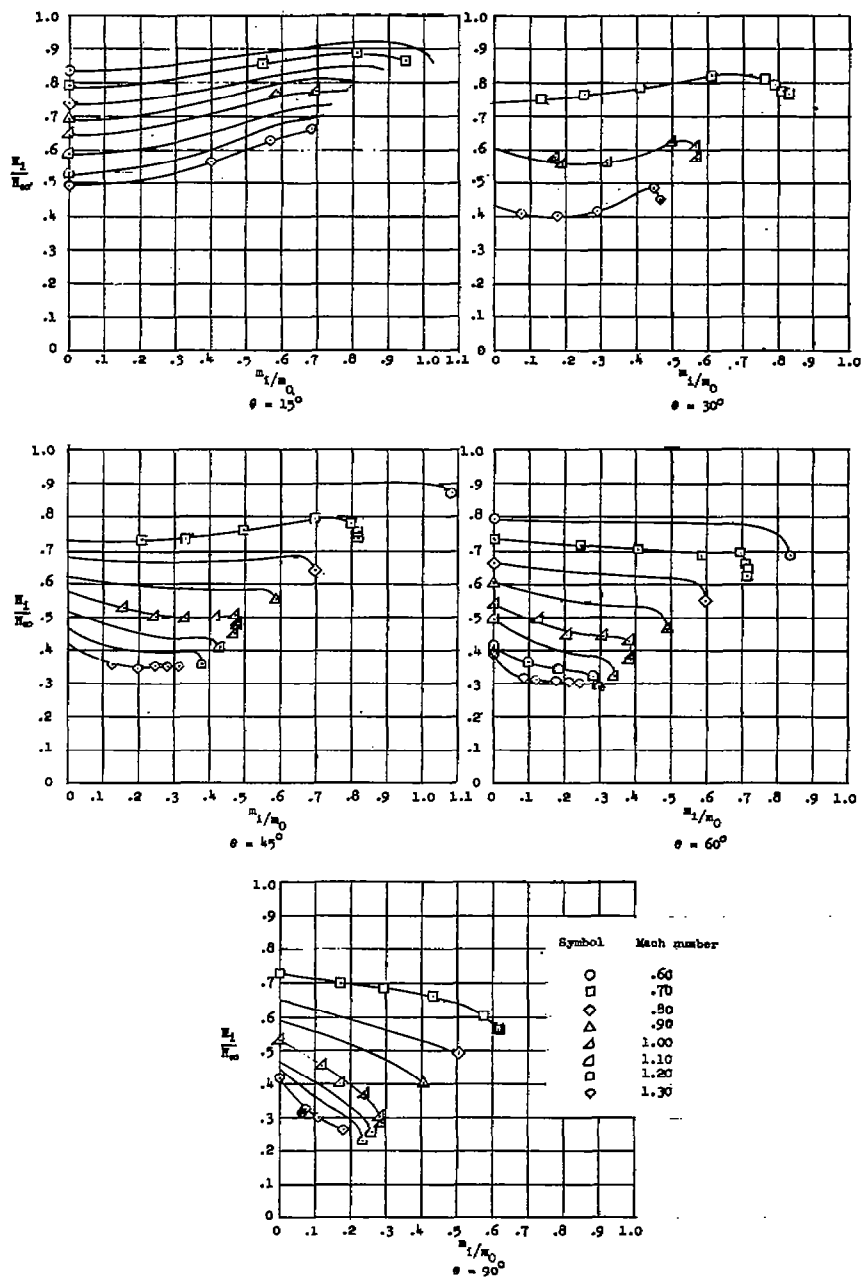
(h) Circular scoop inlets; varying  $\psi$ ;  $L/D = 6.8$ .

Figure 6.- Concluded.



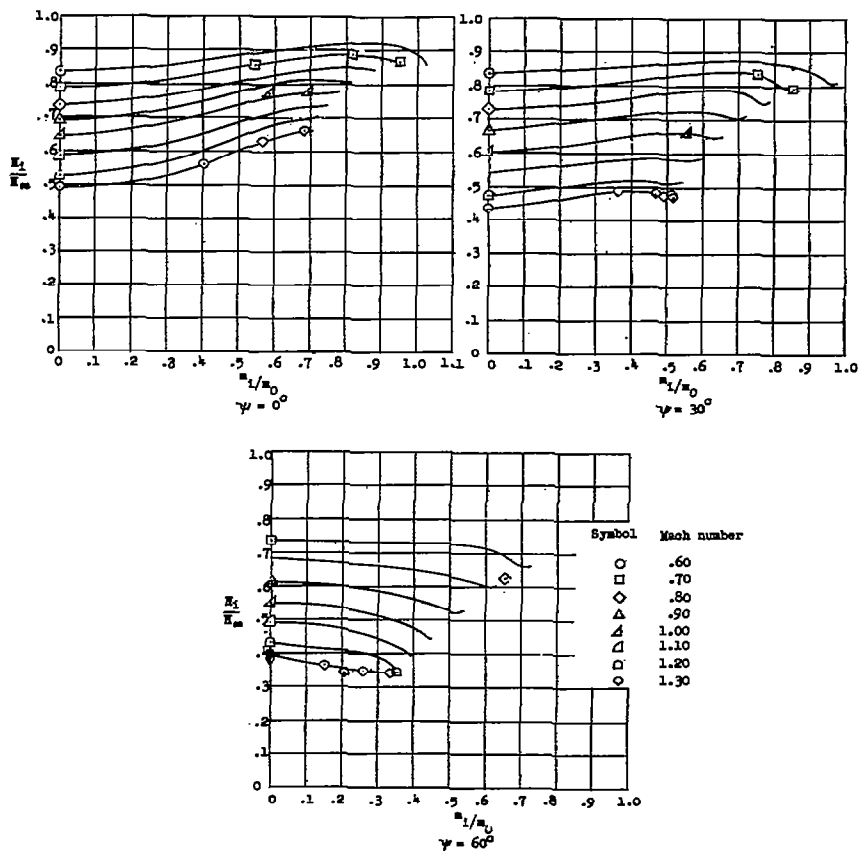
(a) Flush circular inlet; varying  $L/D$ ;  $\theta = 90^\circ$ .

Figure 7.- Variation of inlet total-pressure ratio with mass-flow ratio.



(b) Flush circular inlets; varying  $\theta$ ;  $L/D = 5$ ;  $\psi = 0^\circ$ .

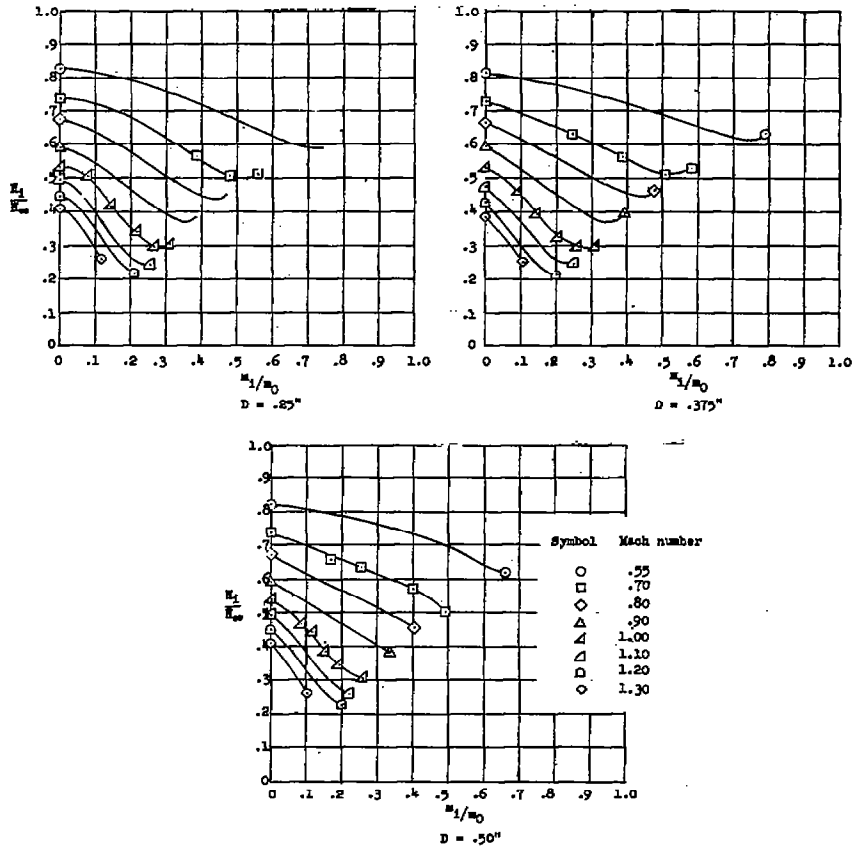
Figure 7.- Continued.



(c) Flush circular inlets; varying  $\psi$ ;  $L/D \approx 5$ ;  $\theta = 15^\circ$ .

Figure 7.- Continued.

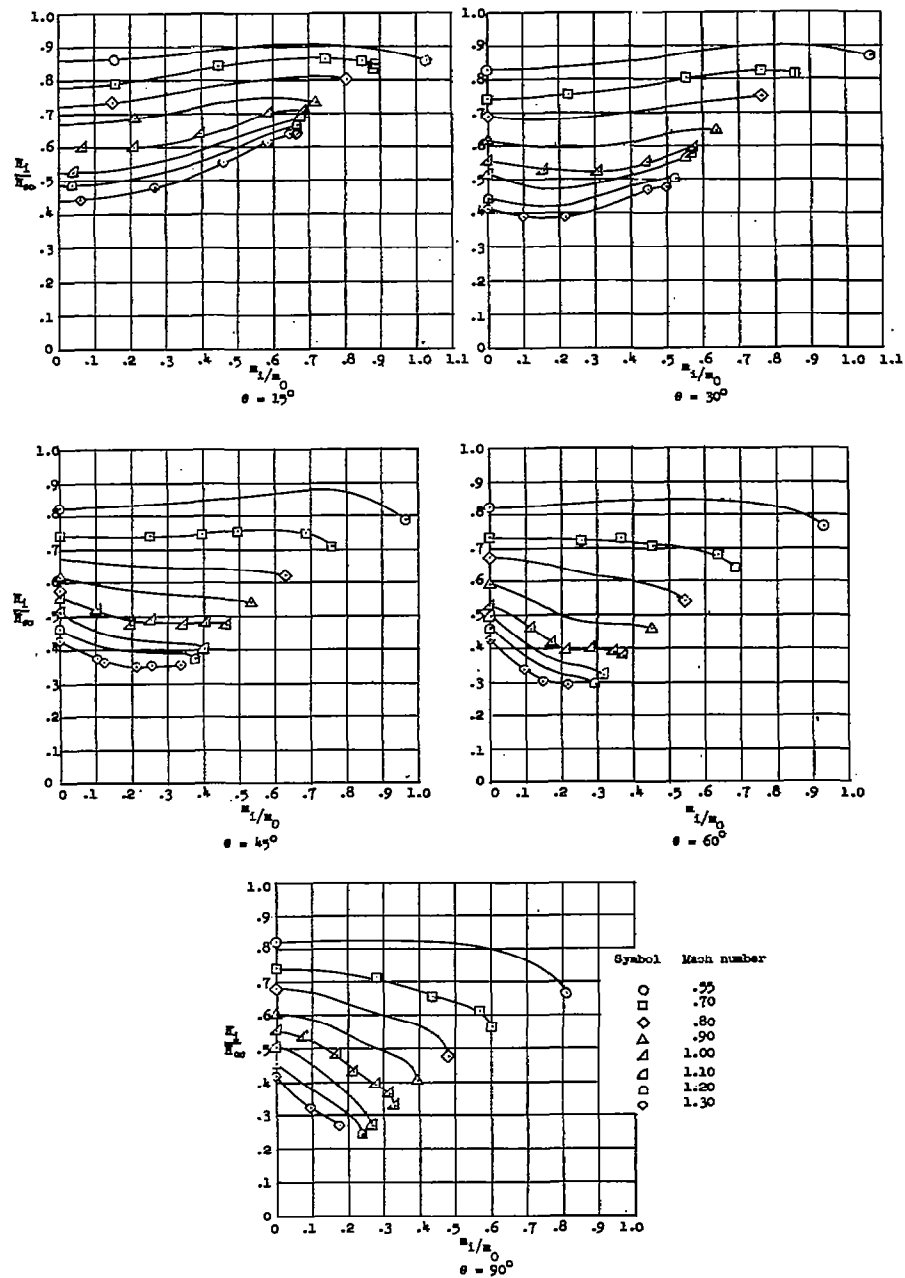
CONFIDENTIAL



(d) Thin-plate inlets;  $t = 1/16$  inch.

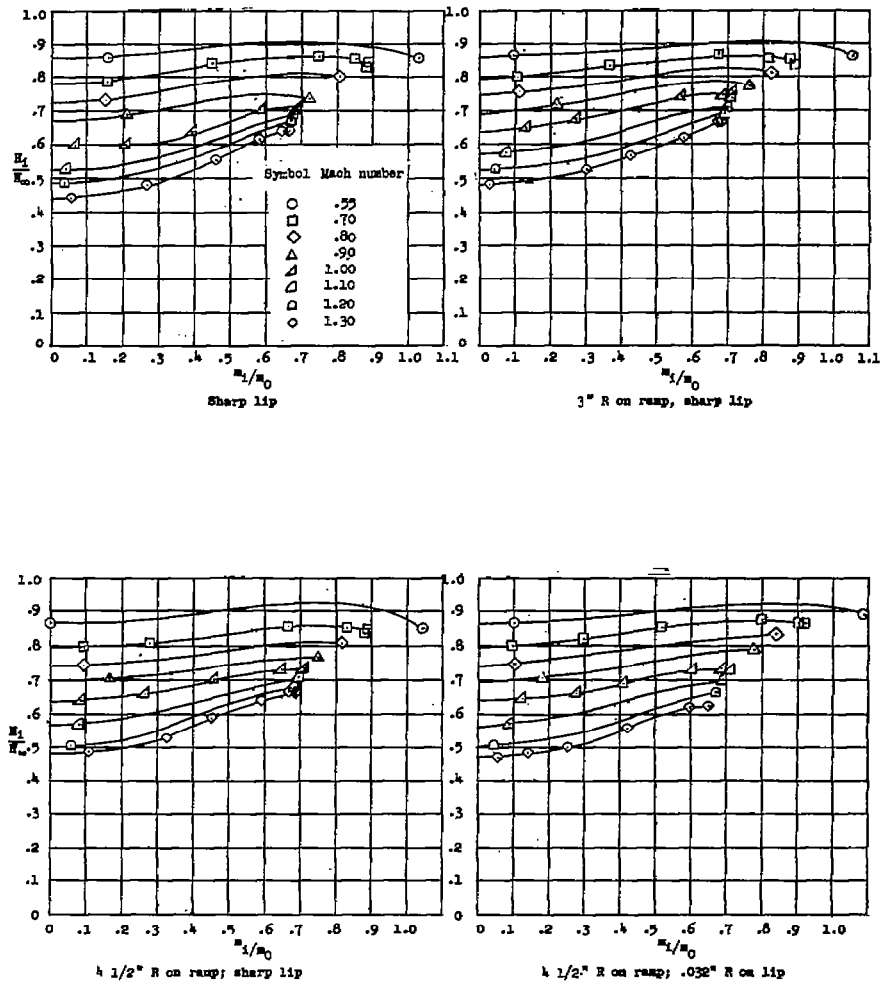
Figure 7.- Continued.

CONFIDENTIAL



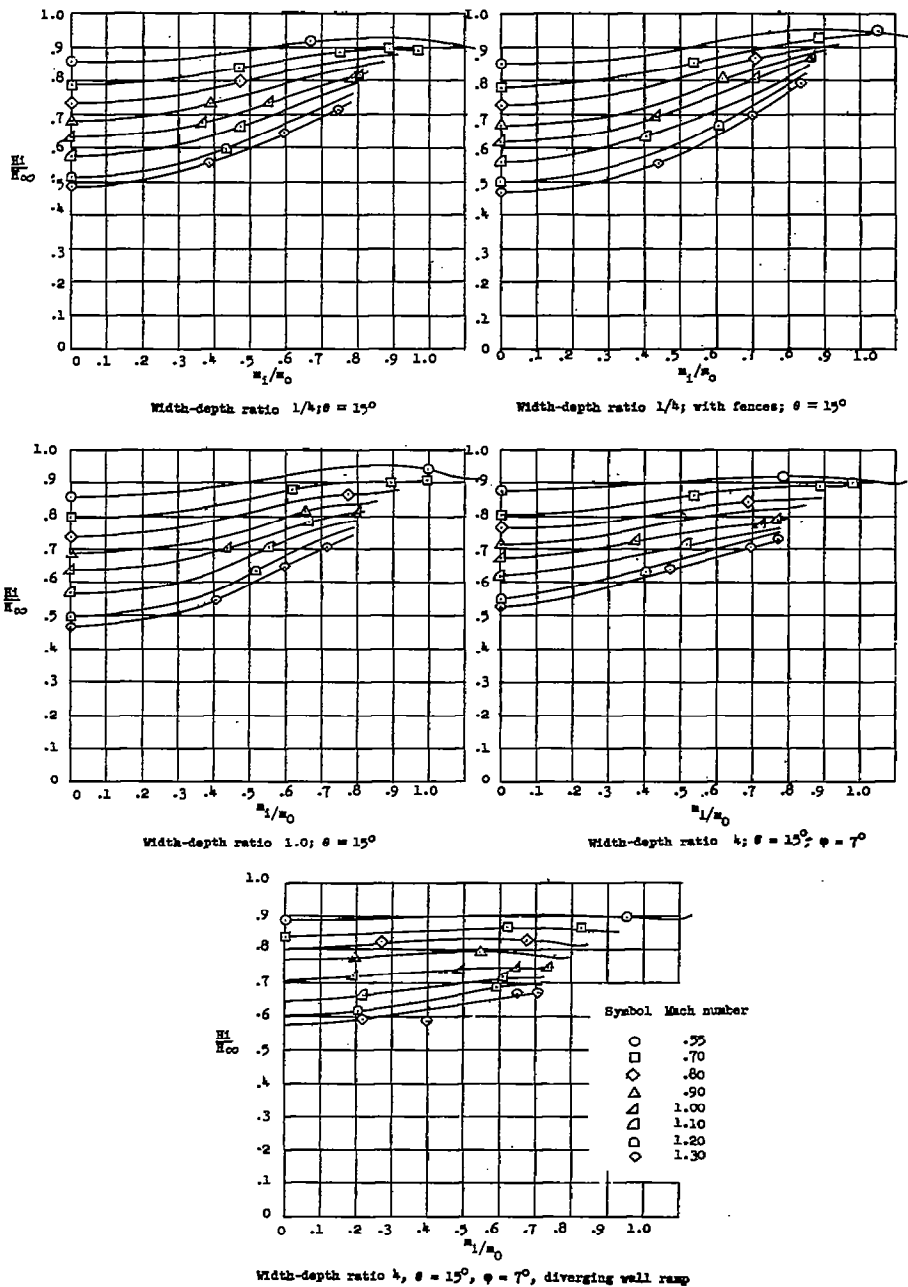
(e) Flush rectangular inlets; varying  $\theta$ ;  $L/D = 5$ ;  $\psi = 0^\circ$ ; width-depth ratio 4.

Figure 7.- Continued.



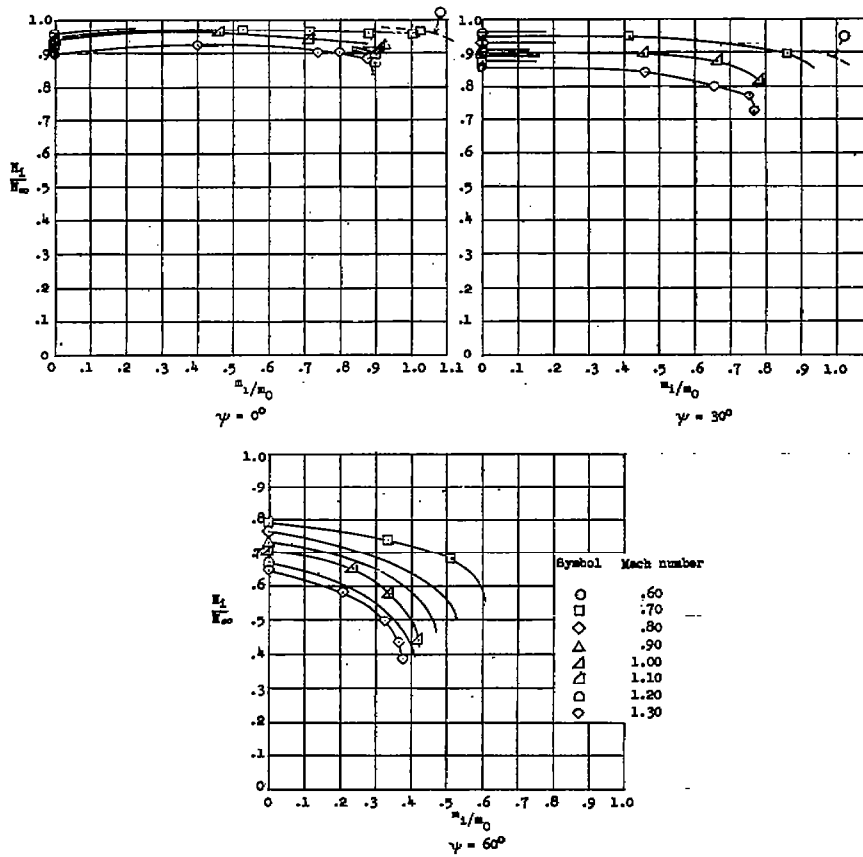
(f) Flush rectangular inlets; varying entrance geometry;  $\theta = 15^\circ$ ;  $L/D = 5$ ;  
 $\psi = 0^\circ$ ; width-depth ratio 4.

Figure 7.- Continued.



(g) Flush rectangular inlets; varying width-depth ratio and  $\phi$ ;  $L/D = 5$ ;  $\psi = 0$ .

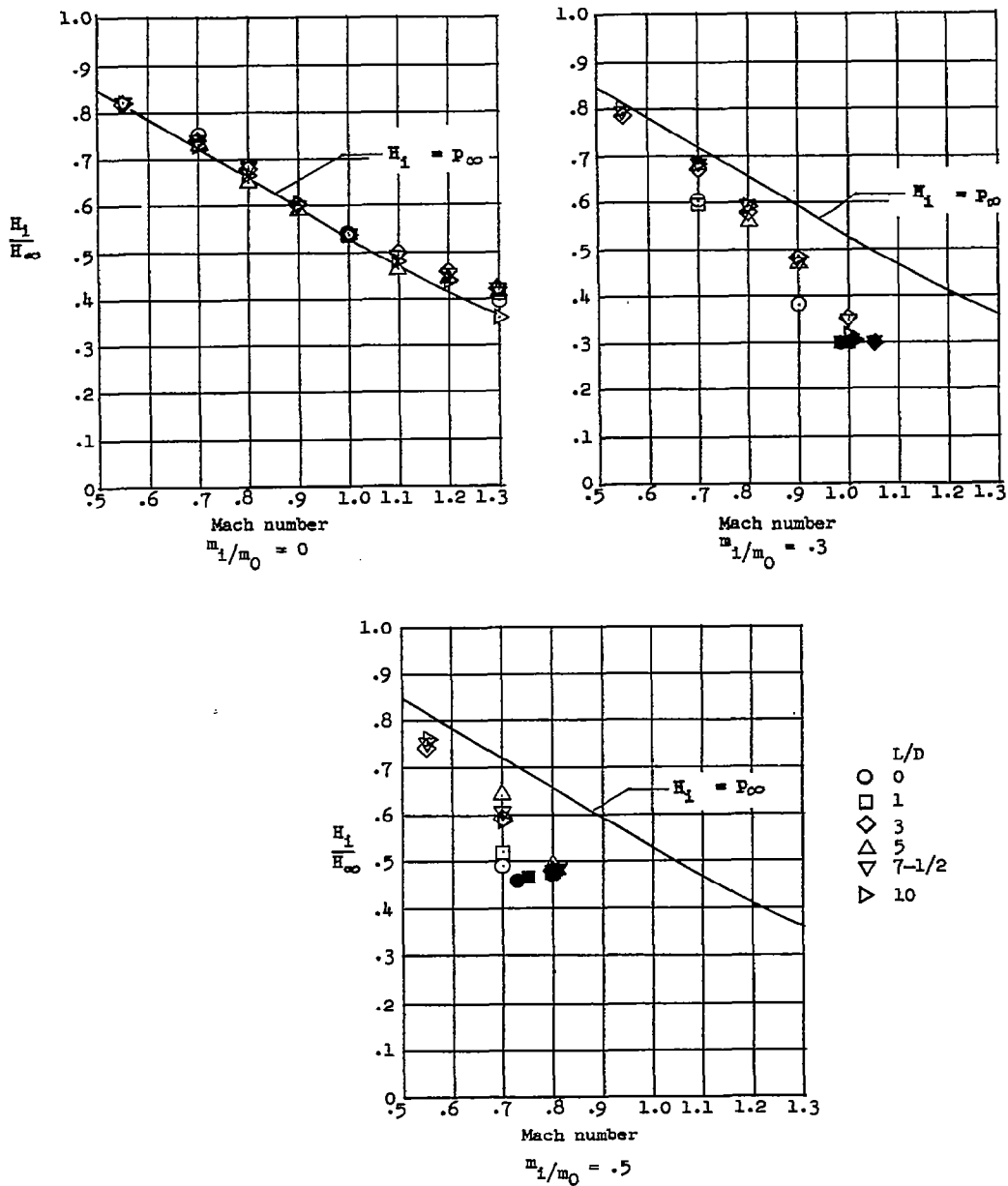
Figure 7.- Continued.



(h) Circular scoop inlets; varying  $\psi$ ;  $L/D = 6.8$ .

Figure 7.- Concluded.

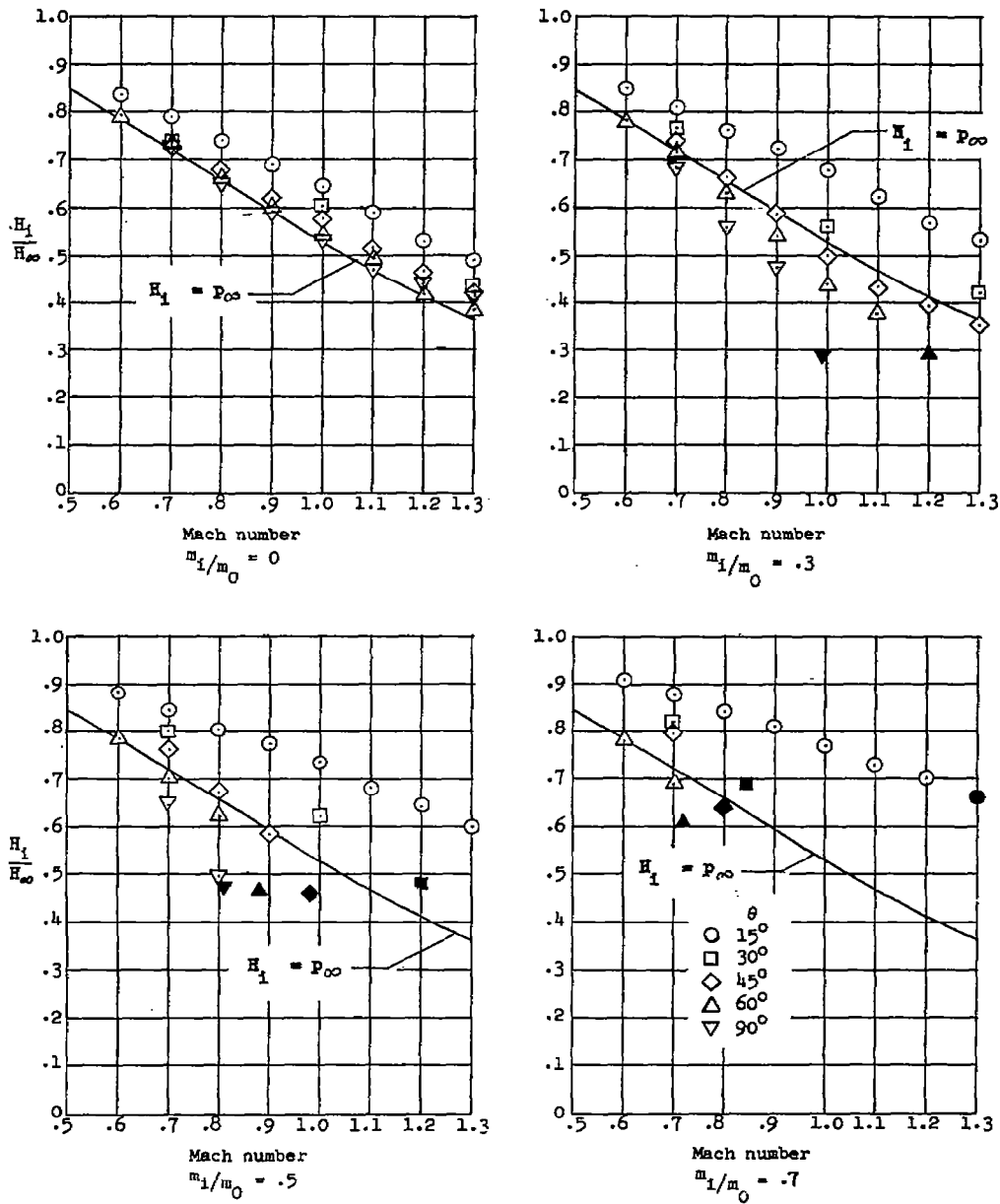
~~CONFIDENTIAL~~



(a) Flush circular inlets; varying  $L/D$ ;  $\theta = 90^\circ$ .

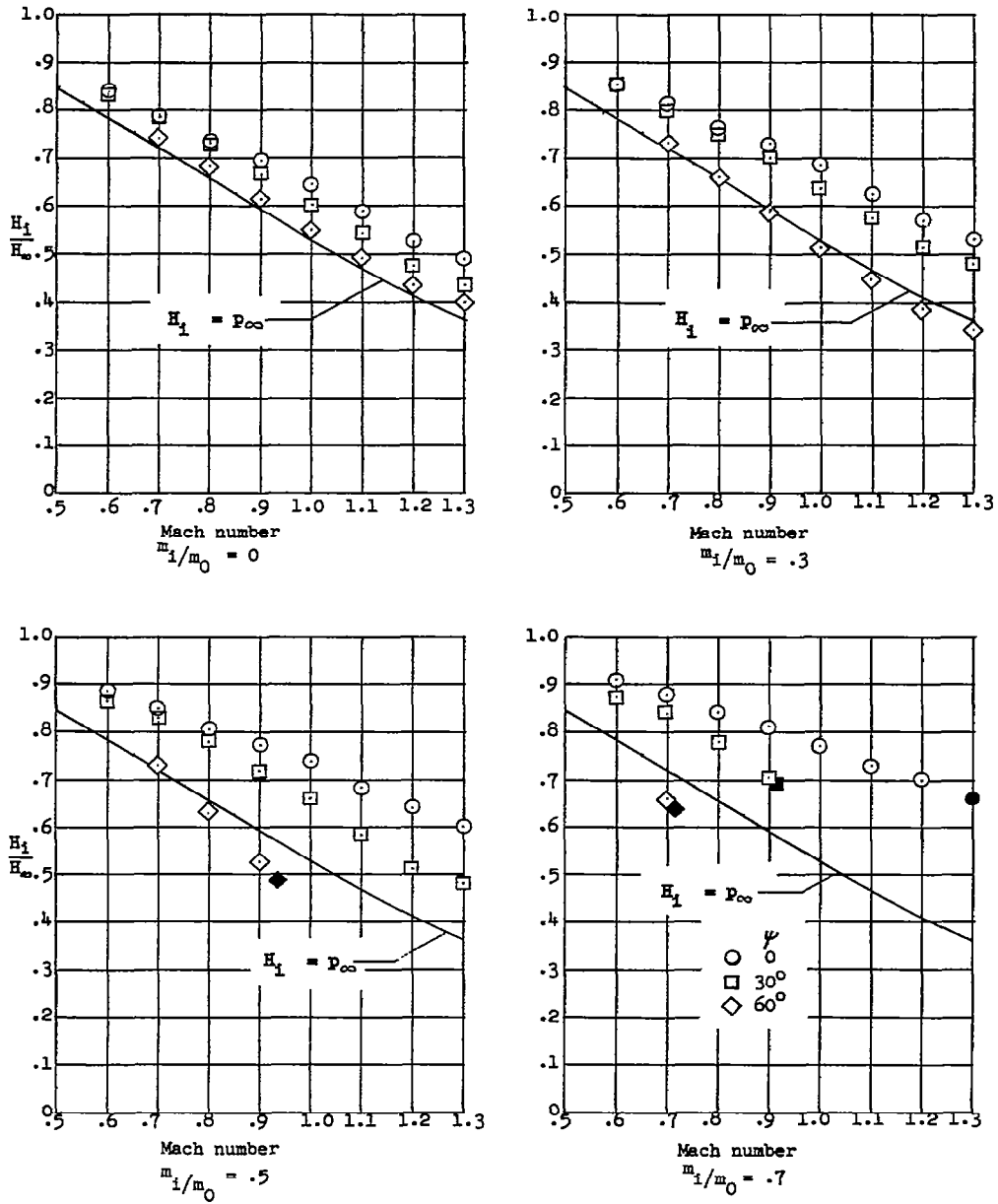
Figure 8.- Variation of total-pressure ratio with Mach number for several values of mass-flow ratio.

~~CONFIDENTIAL~~



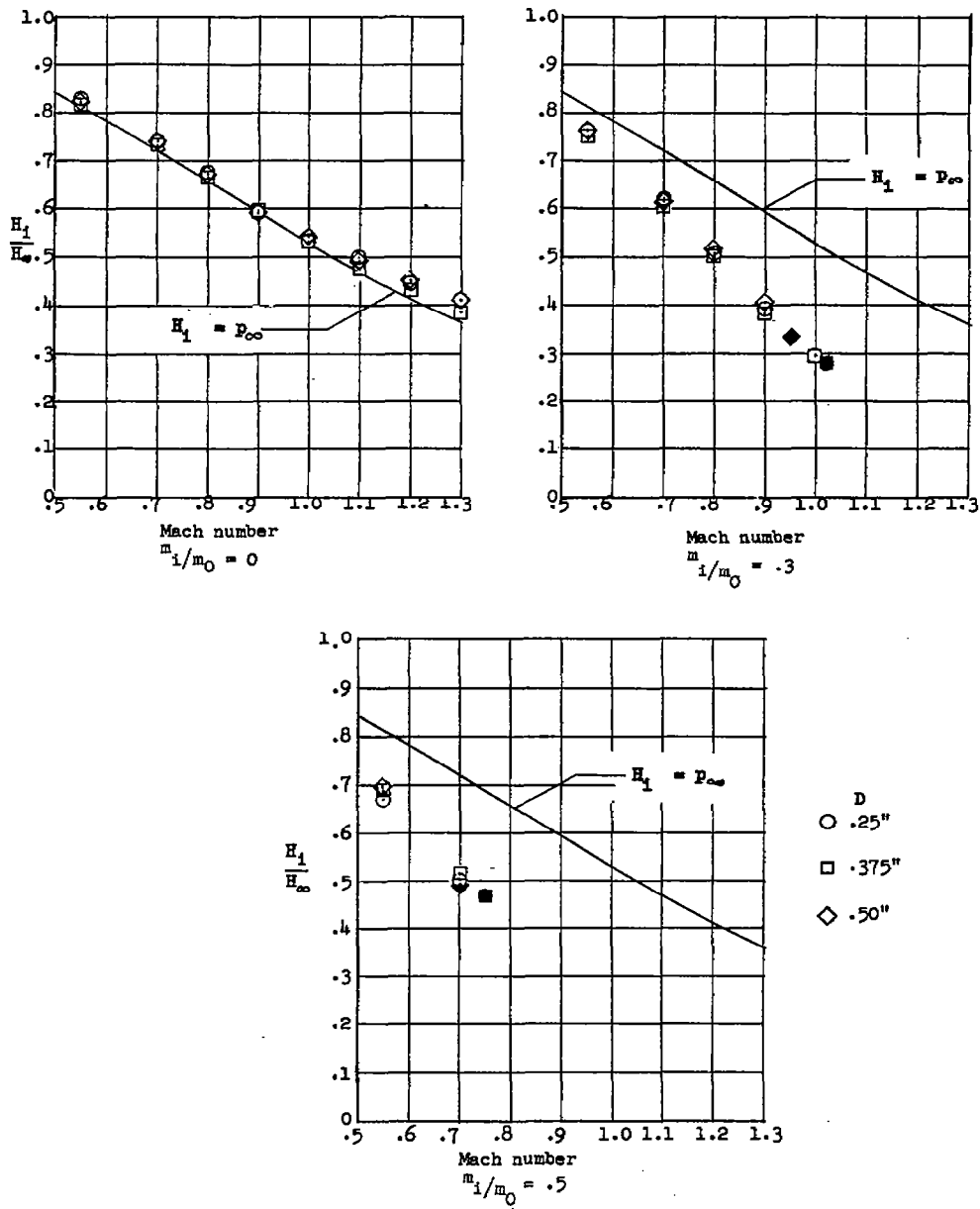
(b) Flush circular inlets; varying  $\theta$ ;  $L/D = 5$ ;  $\psi = 0^\circ$ .

Figure 8.- Continued.



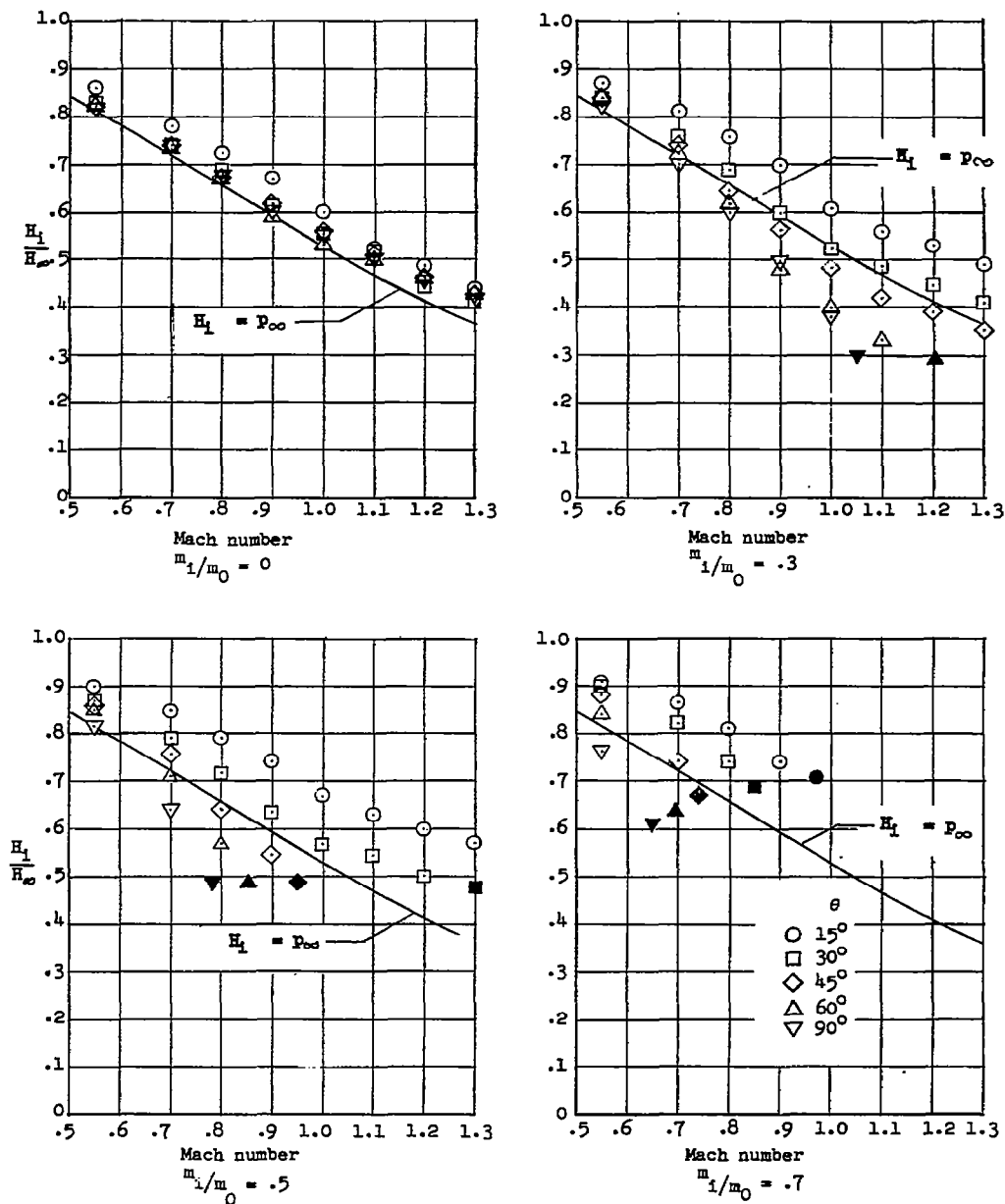
(c) Flush circular inlets; varying  $\psi$ ;  $L/D = 5$ ;  $\theta = 15^\circ$ .

Figure 8.- Continued.



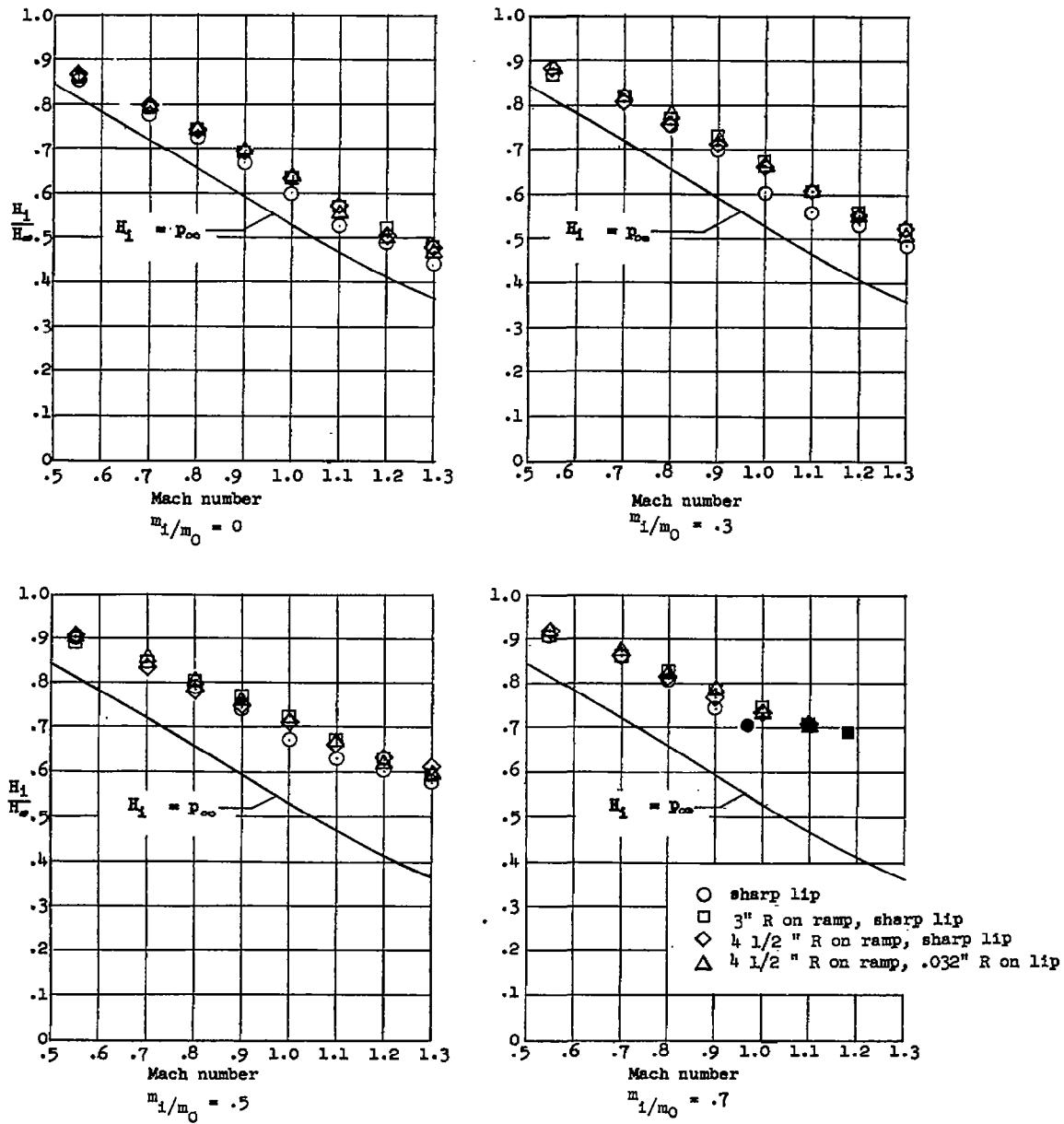
(d) Thin-plate inlets;  $t = 1/16$  inch.

Figure 8.- Continued.



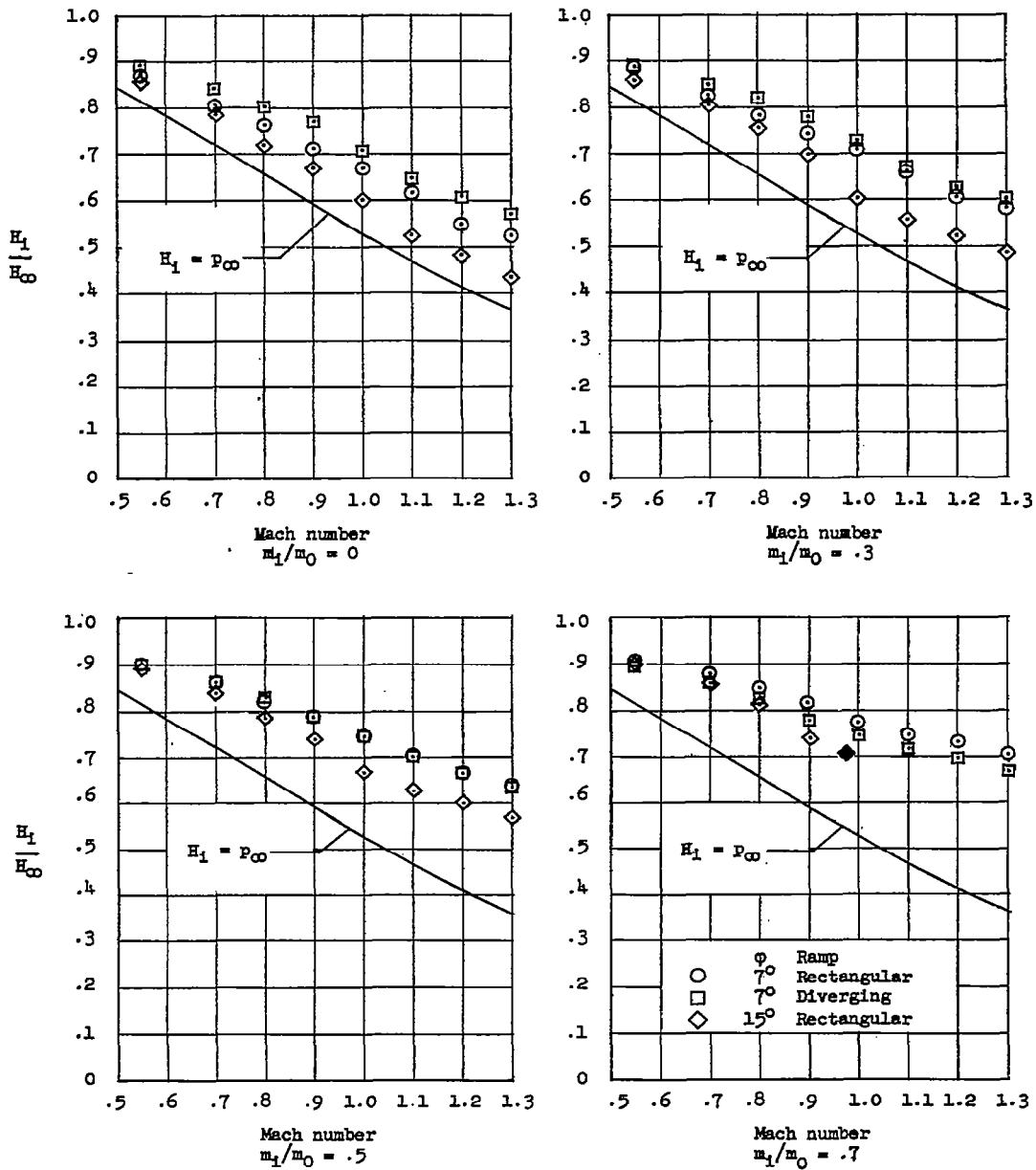
(e) Flush rectangular inlets; varying  $\theta$ ;  $L/D = 5$ ;  $\psi = 0^\circ$ ; width-depth ratio 4.

Figure 8.- Continued.



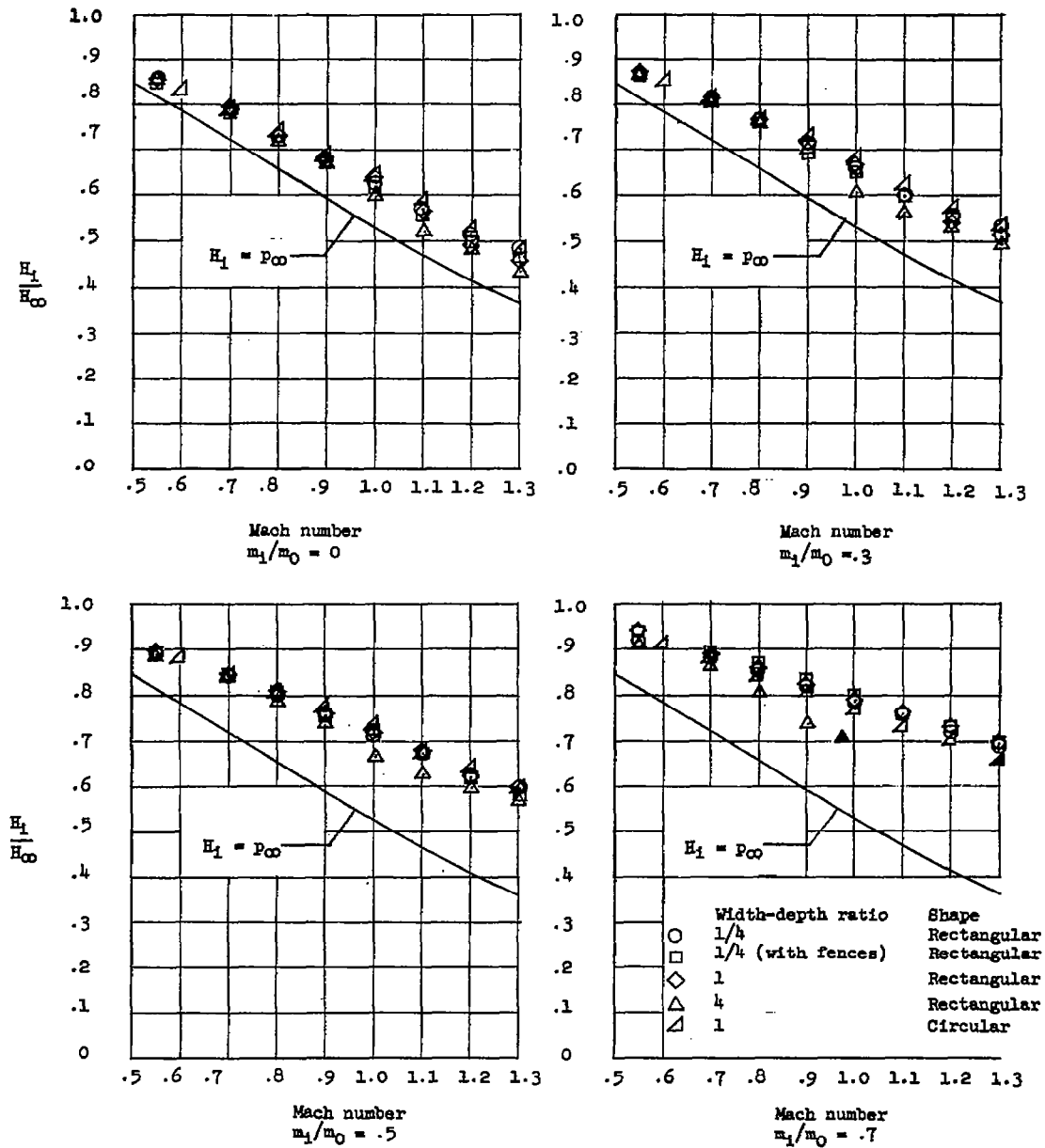
(f) Flush rectangular inlets; varying inlet geometry;  $\theta = 15^\circ$ ;  $L/D = 5$ ;  
 $\psi = 0^\circ$ ; width-depth ratio 4.

Figure 8.- Continued.



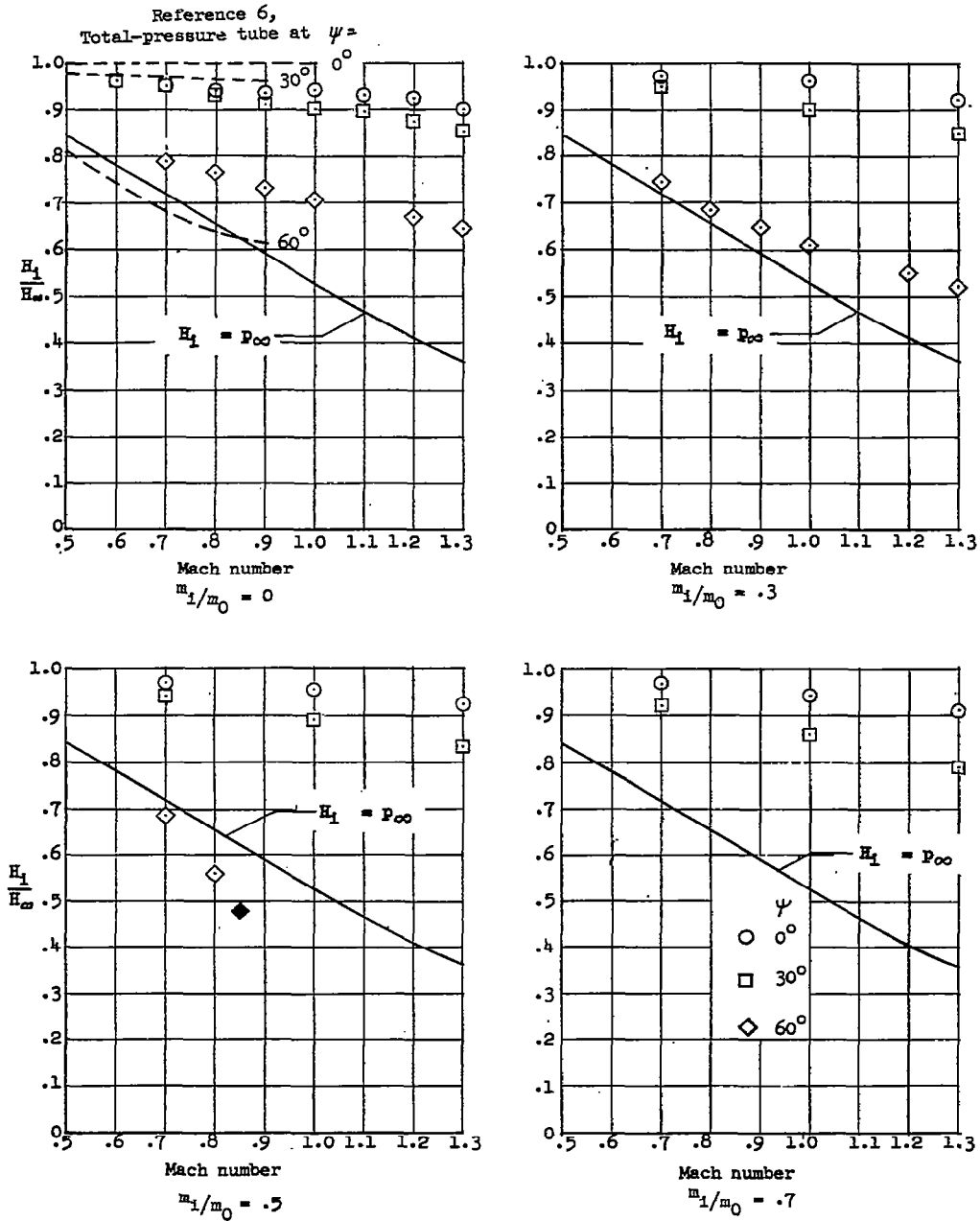
(g) Flush rectangular inlets; varying approach ramp configuration;  $L/D = 5$ ;  $\theta = 15^\circ$ ;  $\psi = 0^\circ$ ; width-depth ratio 4.

Figure 8.- Continued.



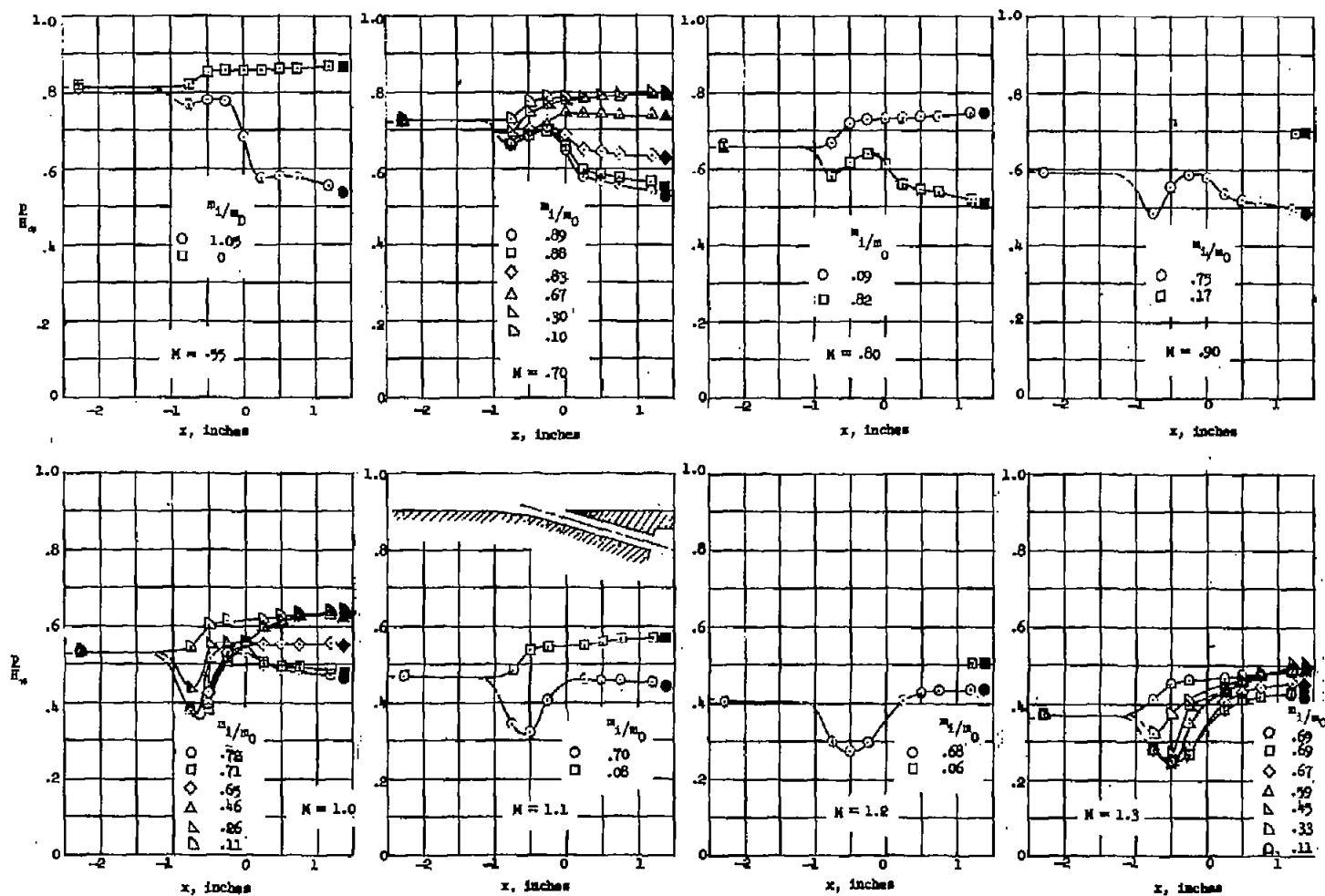
(h) Flush inlets; varying width-depth ratio;  $L/D = 5$ ;  $\psi = 0^\circ$ ;  $\theta = 15^\circ$ .

Figure 8.- Continued.



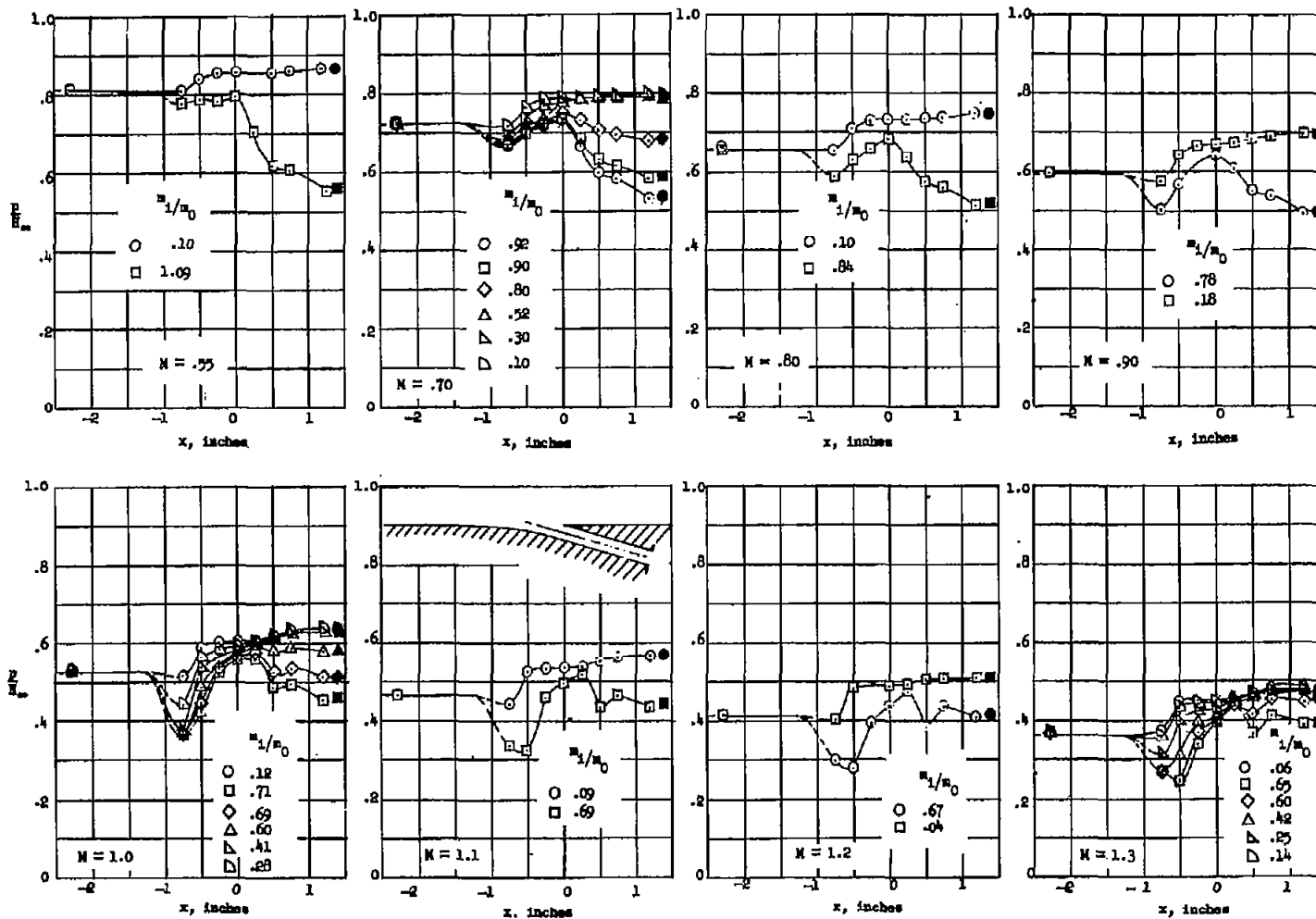
(i) Circular scoop inlets; varying  $\psi$ ;  $L/D = 6.8$ .

Figure 8.- Concluded.



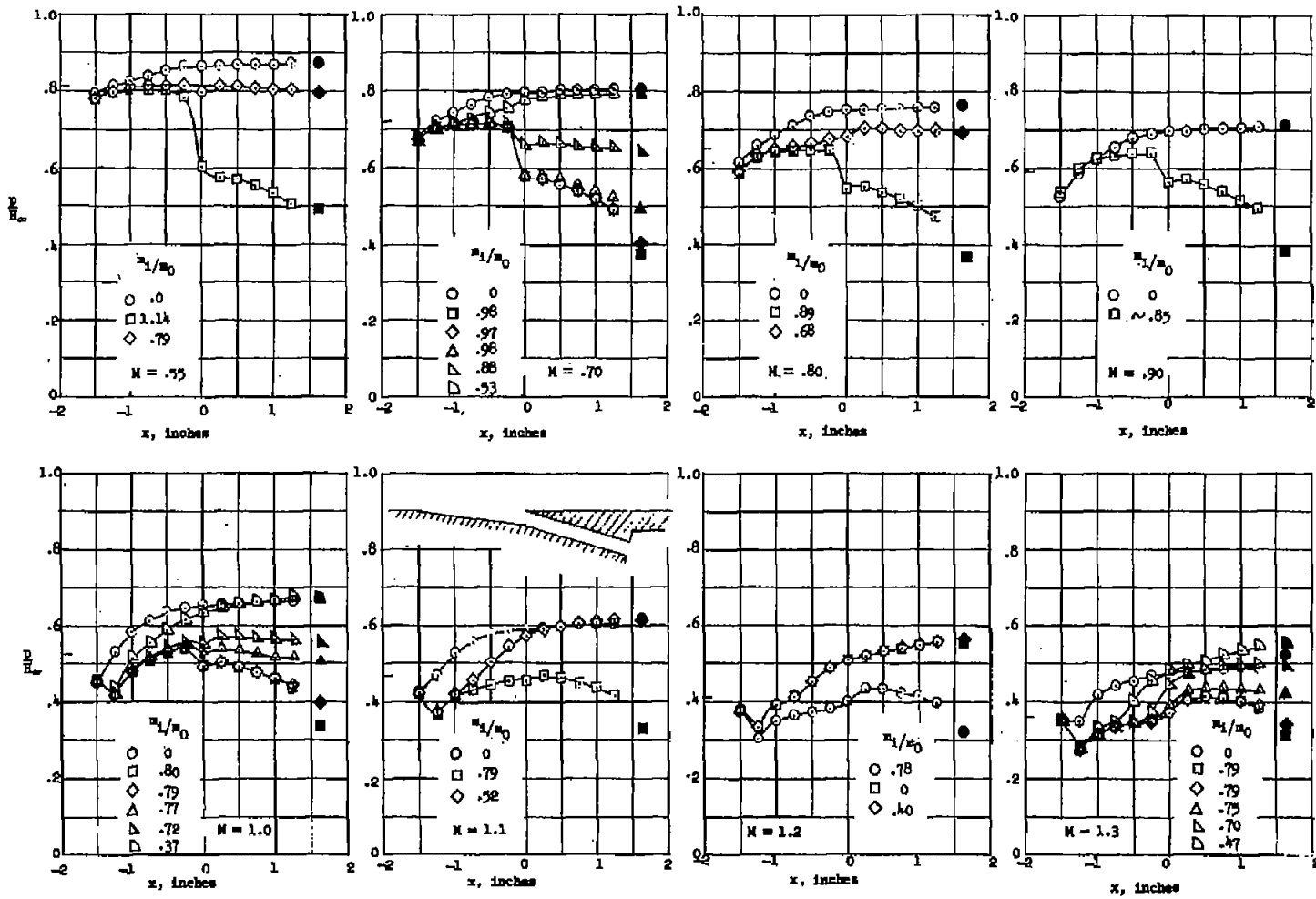
(a) Rectangular inlet; width-depth ratio 4;  $\theta = 15^\circ$ ;  $\psi = 0^\circ$ ;  $1/2$ -inch radius on ramp; sharp lip.

Figure 9.- Static-pressure distributions on ramp and in the inlet passage.



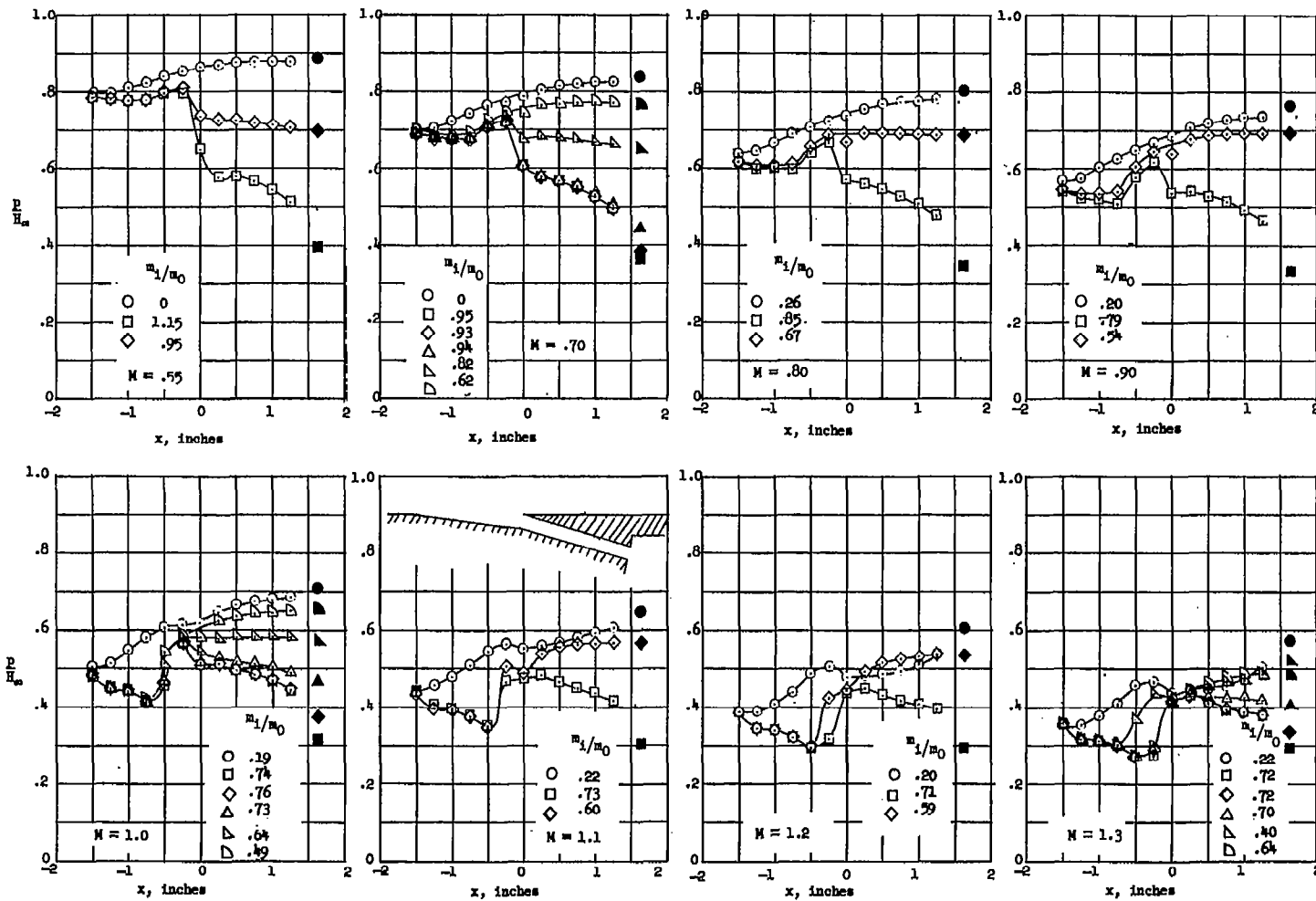
(b) Rectangular inlet; width-depth ratio 4;  $\theta = 15^\circ$ ;  $\psi = 0^\circ$ ;  $4\frac{1}{2}$ -inch radius on ramp; 0.032-inch radius on lip.

Figure 9.- Continued.



(c) Rectangular inlet; width-depth ratio 4;  $\theta = 15^\circ$ ;  $\phi = 7^\circ$ ;  $\psi = 0^\circ$ .

Figure 9.- Continued.



(d) Rectangular inlet; width-depth ratio 4;  $\theta = 15^\circ$ ;  $\phi = 7^\circ$ ;  $\psi = 0^\circ$ ; diverging wall ramp.

Figure 9.- Concluded.